Cell

Article

Product Binding Enforces the Genomic Specificity of a Yeast Polycomb Repressive Complex

Phillip A. Dumesic,[1] Christina M. Homer,[1] James J. Moresco,[2] Lindsey R. Pack,[3] Erin K. Shanle,[4] Scott M. Coyle,[1] Brian D. Strahl,[4] Danica G. Fujimori,[3] John R. Yates III,[2] and Hiten D. Madhani[1,*]

[1]Department of Biochemistry and Biophysics, University of California, San Francisco, San Francisco, CA 94158, USA
[2]Department of Chemical Physiology, The Scripps Research Institute, La Jolla, CA 92037, USA
[3]Department of Cellular and Molecular Pharmacology, University of California, San Francisco, CA 94158, USA
[4]Department of Biochemistry and Biophysics, University of North Carolina School of Medicine, Chapel Hill, NC 27599, USA
*Correspondence: hitenmadhani@gmail.com
http://dx.doi.org/10.1016/j.cell.2014.11.039

SUMMARY

We characterize the Polycomb system that assembles repressive subtelomeric domains of H3K27 methylation (H3K27me) in the yeast *Cryptococcus neoformans*. Purification of this PRC2-like protein complex reveals orthologs of animal PRC2 components as well as a chromodomain-containing subunit, Ccc1, which recognizes H3K27me. Whereas removal of either the EZH or EED ortholog eliminates H3K27me, disruption of mark recognition by Ccc1 causes H3K27me to redistribute. Strikingly, the resulting pattern of H3K27me coincides with domains of heterochromatin marked by H3K9me. Indeed, additional removal of the *C. neoformans* H3K9 methyltransferase Clr4 results in loss of both H3K9me and the redistributed H3K27me marks. These findings indicate that the anchoring of a chromatin-modifying complex to its product suppresses its attraction to a different chromatin type, explaining how enzymes that act on histones, which often harbor product recognition modules, may deposit distinct chromatin domains despite sharing a highly abundant and largely identical substrate—the nucleosome.

INTRODUCTION

The Polycomb (Pc) system plays critical roles in eukaryotic biology by triggering the deposition of facultative heterochromatin. This type of chromatin is associated with two conserved protein complexes: PRC2, whose catalytic subunit (EZH2 in mammals and E(z) in *Drosophila*) is a histone H3 lysine 27 methyltransferase; and PRC1, which mediates chromatin compaction and histone H2A ubiquitylation (Simon and Kingston, 2009). PRC1 also contains a chromodomain protein, CBX/Pc, which recognizes H3K27 methylation (H3K27me). First identified in *Drosophila* as a mechanism responsible for epigenetic memory of developmental gene expression states, the Polycomb system is now appreciated to play key roles in mammalian development as well (Aloia et al., 2013; Steffen and Ringrose, 2014). Diverse additional biological roles have been ascribed to the system in other contexts, ranging from the control of DNA elimination in ciliates to the coupling of flowering and cold exposure in plants (Chalker et al., 2013; Song et al., 2012). Significantly, Polycomb plays a widespread role in human cancers. Redistribution of H3K27me domains has been observed in cancer genomes (Bender et al., 2013; Popovic et al., 2014), as have mutations in Polycomb system components including EZH2, the H3K27 demethylase KDM6A/Utx, and in histone genes at the lysine 27 residue itself (Plass et al., 2013). These findings have driven efforts to develop chemotherapeutics aimed at the Polycomb system.

The appropriate functioning of facultative heterochromatin requires its restricted deposition at the proper genomic sites. In *Drosophila*, DNA sequence elements called Polycomb response elements are bound by specific DNA-binding proteins that themselves recruit PRC2 (Simon and Kingston, 2013). In mammals, however, analogous elements have yet to be identified. PRC2 localization and activity have been suggested to instead be controlled by a diverse set of inputs including DNA-binding proteins, DNA GC content, noncoding RNAs, nucleosome spacing, and numerous histone posttranslational modifications (Klose et al., 2013; Margueron and Reinberg, 2011; Simon and Kingston, 2013). Further complicating the picture, recent studies have shown that H2A ubiquitylation can recruit PRC2 in order to promote H3K27me, thereby challenging the model that PRC2 recruitment acts upstream of PRC1 (Blackledge et al., 2014; Cooper et al., 2014). Thus, the mechanisms that establish H3K27me domains remain highly enigmatic.

A tractable yeast Polycomb system would enhance investigations of this evolutionarily conserved mechanism. Unfortunately, genes encoding PRC2 components were lost during the evolution of highly developed yeast systems such as *S. cerevisiae* and *S. pombe* (Shaver et al., 2010), precluding either from serving as such a model. Here, we identify and characterize a PRC2 complex in a budding yeast, *Cryptococcus neoformans*, and describe a function for H3K27me recognition in the accurate assembly of this type of heterochromatin. We show that the *C. neoformans* EZH2 ortholog acts to deposit H3K27me3 in subtelomeric regions, silencing gene expression across large domains. This activity requires a PRC2-like complex whose

subunits include orthologs of metazoan PRC2 components as well as a chromodomain protein that binds specifically to H3K27me marks. Disruption of this binding activity reconfigures the genomic landscape of H3K27me3 to one that strikingly coincides with sites of H3K9me2 heterochromatin. Indeed, we find that this redistribution is entirely dependent on the Clr4 histone methyltransferase that deposits H3K9me2. These results indicate that the binding of PRC2 to its product restrains a latent attraction toward signals that emanate from H3K9me2 domains. Chromodomain-mediated recognition of H3K27me thereby limits the commingling of two distinct types of repressive chromatin. As many chromatin-modifying complexes contain product recognition modules, the principle uncovered here may broadly contribute to the fidelity of genome-regulating enzymes that act upon a highly abundant and grossly identical substrate—the nucleosome.

RESULTS

Subtelomeric Domains Are Repressed by Methylation of Histone H3 on Lysine 27

PRC2 component orthologs have been identified in protists, filamentous fungi, and algae, and in some cases have been linked to repressive H3K27 methylation (Connolly et al., 2013; Jamieson et al., 2013; Liu et al., 2007; Shaver et al., 2010). Because the human fungal pathogen *C. neoformans* encodes genes for such orthologs (Shaver et al., 2010), we investigated the potential for H3K27me in this organism. However, the amino acid sequence of histone H3 in *Cryptococcus* contains an insertion of two amino acids following residue 28 as well as flanking substitutions that are not present in other model eukaryotes, precluding the use of commercial antibodies (Figure 1A). We therefore purified specific antibodies from rabbit polyclonal antiserum raised against a synthetic H3K27me3 peptide that corresponded to the predicted *Cryptococcus* sequence (Extended Experimental Procedures). Dot blot analysis demonstrated that the purified antibody does not cross-react with H3K27me2, H3K9me2/3, or unmodified H3K27 peptides (Figure S1A).

Use of the H3K27me3 antibody for ChIP-seq revealed the presence of this mark in broad domains at every subtelomeric region of the 14 *C. neoformans* chromosomes (Figures 1B and S1B). Although subtelomeres are enriched in repetitive sequences, the H3K27me3 distribution is similar when ChIP-seq analysis is restricted to unique sequences (Figure S1C). Because we observed minimal signal in other regions of the genome (Figure S1B), we focused our analysis on subtelomeres by generating metatelomere plots: all 28 chromosome ends were aligned, after which their average H3K27me3 signal was calculated as a function of chromosomal position and normalized to that of a whole-cell extract (WCE) sample (Figure 1C). Subtelomeric H3K27me3 domains have an average size of 41 kb (Table S1). Importantly, these domains are not observed in cells lacking the putative H3K27 methyltransferase Ezh2 (Figures 1B and 1C).

Given the conserved role of Polycomb in repressing transcription, we examined the effect of H3K27me3 domains on gene expression in *C. neoformans*. When grown in rich media, cells lacking Ezh2 show widespread gene derepression, as determined by RNA-seq: 75 transcripts increase in expression >3-fold as compared to wild-type cells, whereas no transcript except that of *EZH2* itself decreases >3-fold. Most derepressed loci (71%) are within the 41 kb subtelomeric regions identified by H3K27me3 ChIP-seq, despite the fact that these regions make up only 5% of the genome (Figure 1D). In fact, when all genome-wide sites of H3K27me3 signal are assessed (Figure S1D), most sites lie in subtelomeric regions and no sites greater than 50 kb from a chromosome end are associated with transcript derepression. Thus, the nonsubtelomeric transcripts repressed by Ezh2 are unlikely to be directly regulated by H3K27me3.

Our findings indicate that H3K27me3 in *C. neoformans* depends on the presence of the *EZH2* gene product. To test the functional importance of this histone residue, we incorporated a K27A mutation into histone H3, which is encoded by a single-copy gene in *C. neoformans*. Cells harboring the *h3-K27A* mutation show subtelomeric transcript derepression as much as 60-fold, as assessed by RT-qPCR analysis of five transcripts identified by RNA-seq to be elevated in *ezh2Δ* cells (Figure 1E). The phenotype of an *h3-K27A ezh2Δ* double mutant is indistinguishable from that of each single mutant, suggesting that Ezh2, in its gene silencing role, acts via H3K27. Next, we generated strains that encoded Ezh2 SET domain mutations predicted to eliminate its catalytic activity (Tan et al., 2014). These mutations, which have little (681-689Δ) or no (Y721A) effect on Ezh2 protein levels, recapitulate the high degree of subtelomeric transcript derepression seen in *ezh2Δ* cells (Figures 1F and 1G). Our results support a model in which Ezh2 deposits broad domains of repressive subtelomeric H3K27me3.

A Yeast PRC2-like Complex

The activity of metazoan EZH2 is controlled extensively by inputs from the other PRC2 subunits (O'Meara and Simon, 2012). To determine whether a similar regulatory logic might exist in *C. neoformans*, we investigated the protein-interaction partners of Ezh2 in this system. We generated cells expressing CBP-2xFLAG-tagged Ezh2 from its normal chromosomal site, then isolated it by tandem affinity purification and identified its copurifying proteins by mass spectrometry. This purification yielded Ezh2 itself as well as four additional proteins, two of which are orthologs of metazoan PRC2 components (Figures 2A, 2B, and see below). We subsequently tagged and affinity-purified each of these four proteins: Eed1, Msl1, Bnd1, and Ccc1 (Figures 2A and 2B). Purifications of these proteins consistently yielded the original five Ezh2-associated proteins, suggesting the existence of a core PRC2-like protein complex (Figure 2C). The other proteins in the interaction network, which associated with only a subset of the core PRC2 components, may represent more loosely associated factors. Alternatively, these proteins may interact with individual PRC2 components in PRC2-independent contexts.

The members of the putative PRC2-like complex include orthologs of metazoan PRC2 components as well as additional factors (Figure 2D and Extended Experimental Procedures). Ezh2 is the H3K27 methyltransferase and Eed1 is an ortholog of EED/Esc, a WD40 repeat protein that binds directly to EZH2/E(z) and stimulates EZH2/E(z) activity. Msl1 is a fungal ortholog of RbAp46/48/Nurf55, a WD repeat protein that associates with

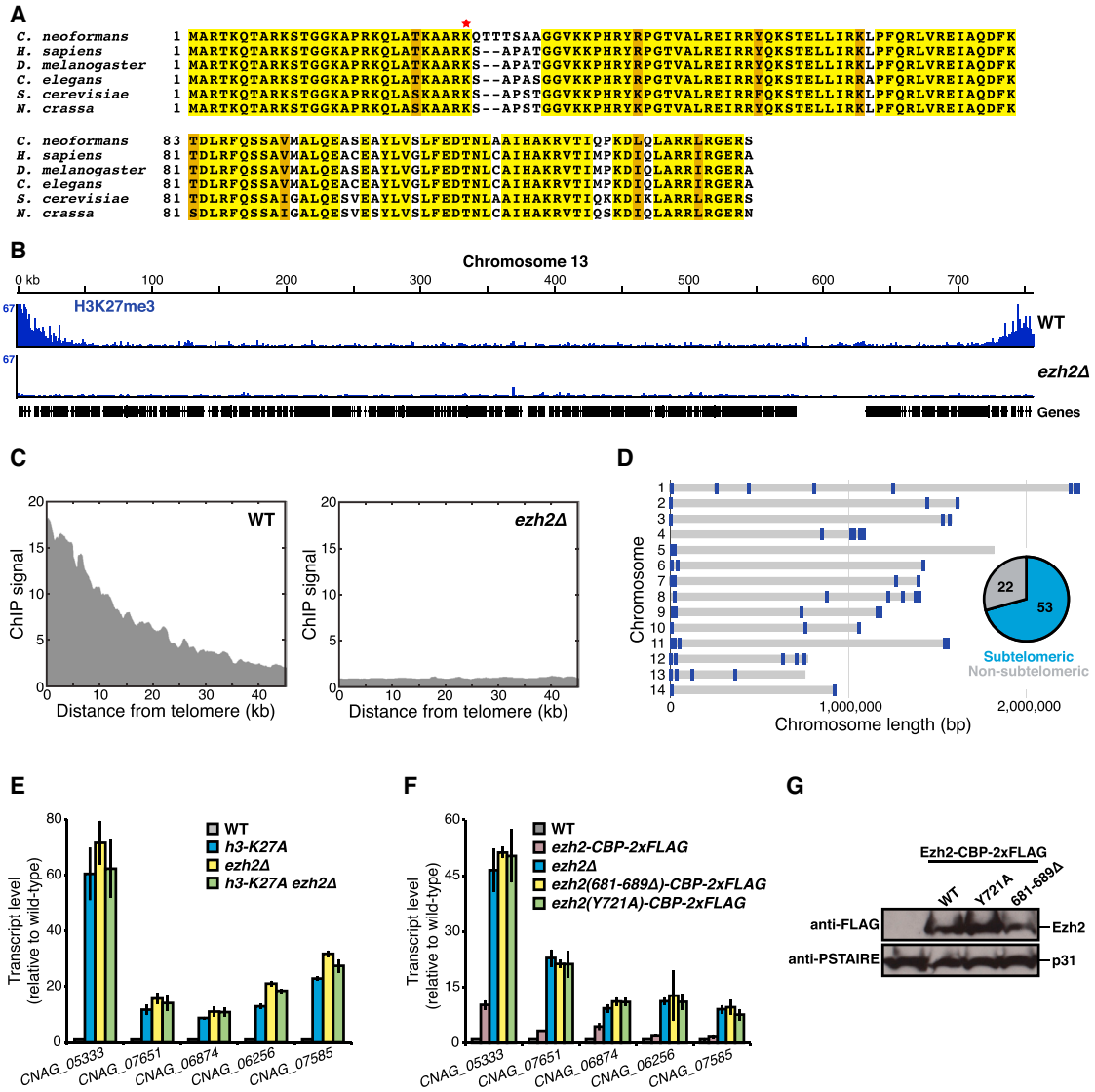

Figure 1. *C. neoformans* Ezh2 Deposits Broad, Subtelomeric Domains of Repressive H3K27me3 Heterochromatin

(A) Alignment of histone H3 protein sequences in eukaryotic model systems. Red star indicates lysine 27, a substrate of Ezh2.

(B) ChIP-seq traces of H3K27me3 signal across the representative chromosome 13 in wild-type or *ezh2Δ* cells. Other chromosomes are shown in Figure S1B.

(C) Average subtelomeric H3K27me3 signal, as measured by ChIP-seq. ChIP signal at all 28 subtelomeric regions was averaged, normalized to a WCE sample, and plotted as a function of distance from chromosome end.

(D) Chromosomal location of transcripts whose levels are elevated >3-fold in the absence of Ezh2, as assessed by RNA-seq. The proportion of these loci within the 41 kb subtelomeric H3K27me3 domains is indicated.

(E) Transcript levels of five Ezh2 target genes in the context of histone H3 or Ezh2 mutations, as assessed by RT-qPCR and normalized to 18S rRNA levels. Error bars represent SD.

(F) Transcript levels of five Ezh2 target genes in the context of Ezh2 SET domain mutations, as assessed by RT-qPCR and normalized to 18S rRNA levels. Error bars represent SD.

(G) Expression level of Ezh2 SET domain mutants, as assessed by immunoblot using the antibodies indicated at left. p31 serves as a loading control.

See also Figure S1 and Table S1.

PRC2 but is not required for EZH2/E(z) activity and has additional roles in other chromatin-modifying complexes. The remaining components of *C. neoformans* PRC2 are two factors with no clear orthologs in higher eukaryotes: Bnd1, a *b*ig protein with *n*o *d*omains; and Ccc1, a protein that contains a *c*hromodomain and a *c*oiled *c*oil region. Like some other single-celled eukaryotes, *C. neoformans* does not appear to encode an ortholog of the metazoan PRC2 component SUZ12/Su(z)12 in its genome (Shaver et al., 2010).

We used a yeast two-hybrid assay in order to assess pairwise interactions between PRC2 components when expressed in *S. cerevisiae.* We observed that each component interacts with

at least one other complex member, supporting the associations identified by tandem affinity purification (Figure S2A and Table S2). These interactions include one between Eed1 and Ezh2, whose metazoan orthologs bind one another directly in PRC2. Furthermore, two PRC2 components—Bnd1 and Ccc1—display self-interaction, raising the possibility of physical interactions that bridge multiple PRC2 complexes.

To assess the functional roles of each PRC2 subunit, we generated strains lacking each individual factor and tested their ability to silence Ezh2 target loci. Every knockout strain shows derepression of subtelomeric transcripts, as determined by RT-qPCR (Figure 2E). However, their phenotypes differ quantitatively. Cells lacking Ezh2, Eed1, or Bnd1 display equivalent, maximal phenotypes. In contrast, loss of Ccc1 causes a less severe phenotype in which some Ezh2 targets are fully derepressed and others are only partially derepressed. Msl1 mutants display the most minor phenotype: at all tested loci, this protein is only partially required for silencing, consistent with the relatively minor contribution of its ortholog, RbAp46/48/Nurf55, to PRC2-mediated silencing in mammals (O'Meara and Simon, 2012). The physical interactions among the PRC2 components, together with the phenotypes of their corresponding knockouts, suggest that they functionally cooperate, with the individual subunits contributing distinct and separable activities in gene silencing.

Several lines of evidence suggest that Msl1 and Ccc1 play additional roles independent of PRC2. First, Msl1 and Ccc1 physically associate not only with PRC2 components but also with members of the chromatin assembly factor (CAF) complex and multiple histone deacetylase (HDAC) complexes (Figure 2B). Metazoan Msl1 orthologs are involved in similar interactions (Suganuma et al., 2008). Second, both *msl1Δ* and *ccc1Δ* strains exhibit a growth defect, whereas strains lacking any of the other PRC2 components—*ezh2Δ*, *eed1Δ*, and *bnd1Δ*—do not (Table S3). Third, cells lacking Msl1 or Ccc1 demonstrate more widespread gene expression changes than do cells lacking Ezh2, as measured by RNA-seq (Figure 2F). Specifically, Msl1 is required for silencing of approximately half of the Ezh2 target genes, and additionally represses 225 other loci, whereas Ccc1 silences approximately half of the Ezh2 target genes as well as 65 other loci, most of which are coregulated by Msl1.

We tested whether the PRC2-independent factors associated with Msl1 and Ccc1 are involved in repressing PRC2 target loci. We were able to generate knockout strains for a subset of these factors, which we tested by RT-qPCR for their ability to silence subtelomeric transcripts. Loss of Cac2 (of the CAF complex) has no effect on subtelomeric transcript levels, nor does loss of Eza1, Nop1, Hat1, or CNAG_04786 (Figure S2B). A strain lacking Rpd3 (of the Rpd3S and Rpd3L HDAC complexes) displays derepression of a subset of subtelomeric loci, but does not phenocopy the PRC2 component gene knockouts. Notably, however, deletion of the gene encoding an ortholog of *S. pombe* Clr3 leads to a full derepression of subtelomeric genes (Figure S2C), implicating this Class II HDAC ortholog in PRC2 action. Notably, HDAC activity cooperates with PRC2 in metazoan systems, where it removes antagonistic marks such as H3K27 acetylation (Reynolds et al., 2012; Tie et al., 2009).

Together, these data point to the *C. neoformans* PRC2 as a five-protein functional core complex that mediates H3K27me3-dependent gene silencing and shares structural and functional similarities with the metazoan PRC2.

Dissection of PRC2 Function Reveals Subunit Specialization

Having determined that PRC2 components play varying roles in subtelomeric gene repression, we investigated their respective functions in the formation of H3K27me3 domains. We used H3K27me3 ChIP-seq to examine a knockout from each phenotypic group: *ezh2Δ* cells display the maximal transcript derepression phenotype, whereas *ccc1Δ* and *msl1Δ* cells represent two partial phenotypes at the Ezh2 target genes, with the *msl1Δ* phenotype being the more minor of the two. As seen before, *ezh2Δ* cells lack all detectable H3K27me3 signal (Figures 3A and 3B). In contrast, and consistent with its minor transcript phenotype, the *msl1Δ* strain shows only a minor reduction in its subtelomeric H3K27me3 domains: ChIP enrichment is slightly reduced, as is their average size (35 kb versus 41 kb in wild-type, Table S1). Cells lacking Ccc1 have an intermediate phenotype in which subtelomeric H3K27me3 signal is reduced but not eliminated, with small domains (14 kb) still detectable. While these data do not rule out downstream roles for Msl1 and Ccc1, they suggest that these PRC2 components contribute to subtelomeric gene silencing by enabling the formation of appropriately-positioned H3K27me3 domains.

Further examination of the ChIP-seq data revealed a remarkable feature of *ccc1Δ* cells: whereas H3K27me3 signal is reduced at its normal subtelomeric locations, signal is increased at an ectopic site—the centromeres (Figure 3A). Centromeres have not been extensively studied in *C. neoformans*, but consist largely of transposon-derived repeats and correspond to a single broad region on each chromosome that lacks open reading frames (Janbon et al., 2014). H3K27me3 signal is increased at all 14 centromeres in *ccc1Δ* cells, and for some centromeres becomes comparable in magnitude to subtelomeric signal on the same chromosome. To systematically examine centromeric H3K27me3, we generated meta-centromere plots: all centromeres were aligned at their midpoints, after which their average H3K27me3 signal was calculated as a function of chromosomal position and normalized to that of a WCE sample (Figure 3C). Our analysis revealed an increase in centromeric H3K27me3 signal in *ccc1Δ* cells, but not in *msl1Δ* cells.

To quantify the extent of ectopic H3K27me3 deposition, we compared the density of H3K27me3 ChIP-seq signal at its proper sites—subtelomeres—versus centromeres (Figure 3D). As expected, wild-type cells exhibit subtelomeric signal but negligible centromeric signal, whereas *msl1Δ* cells display diminished subtelomeric signal. In contrast, *ccc1Δ* cells show not only a reduction in subtelomeric signal, but also a dramatic increase in centromeric signal (Figure 3D). These findings indicate that multiple PRC2 components are required for the proper spatial distribution of H3K27me3, with Ccc1 specifically being required to prevent an ectopic redistribution of this chromatin mark.

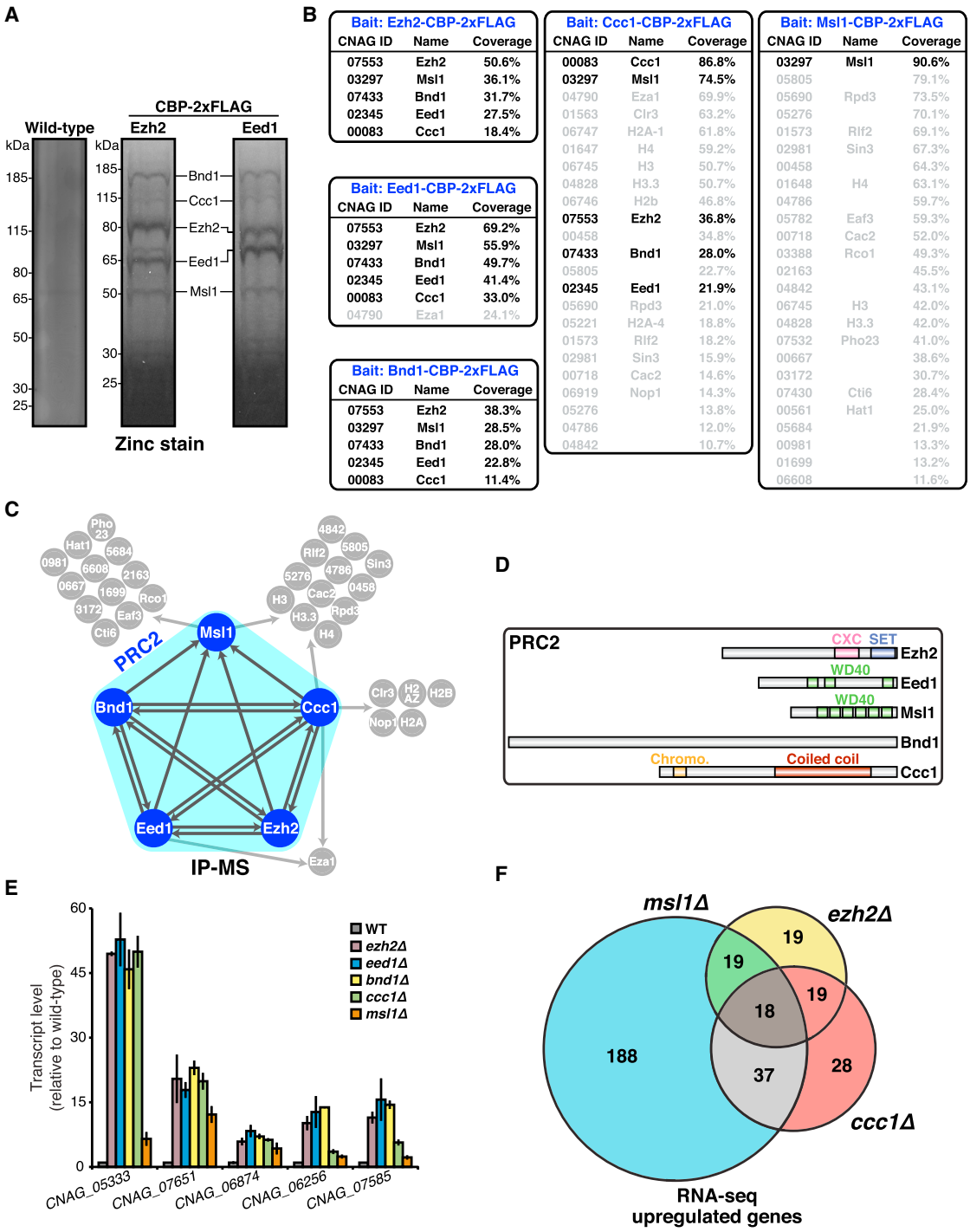

Figure 2. Purification and Functional Characterization of Ezh2-Associated Proteins

(A) Tandem affinity purifications were performed from wild-type (untagged) cells or cells expressing CBP-2xFLAG-tagged Ezh2 or Eed1. Purified protein was resolved by PAGE and visualized by zinc stain. Proteins identified by mass spectrometry analysis of the Ezh2 purification are labeled.

(B) Protein interaction partners of Ezh2 and of each of its associated proteins. Each bait protein was purified by tandem affinity purification and its protein interaction partners were determined by mass spectrometry. Likely contaminants and proteins with <10% sequence coverage have been excluded. Subunits of the putative PRC2 complex are indicated in black type.

(C) Protein interaction network of Ezh2-associated proteins. Each protein shaded in blue was used as bait for a separate IP-MS experiment, and arrows point to its respective associated proteins.

(D) Predicted protein domains of PRC2 subunits.

(legend continued on next page)

Ccc1 Chromodomain Binds H3K27me and Prevents Its Ectopic Deposition

To determine the mechanism by which Ccc1 enforces the correct genomic localization of H3K27me3, we examined its chromodomain, a protein motif that can bind directly to histone methyl-lysine residues (Eissenberg, 2012). First, we recombinantly expressed a truncated fragment of Ccc1 that contains its chromodomain (Figures 4A and S3A). We then tested its capacity to bind histone modifications by using a peptide array representing 384 different histone modification combinations. We observed binding to only eight peptides on the array (Figure 4B). Strikingly, each peptide contains either a H3K27me2 or H3K27me3 modification, implying that the Ccc1 chromodomain is a specific reader of these PRC2-deposited marks. These results were somewhat surprising because the bound peptides correspond to the human H3 sequence, which differs from the *C. neoformans* sequence at residues downstream of K27. The downstream residues may therefore be less important for binding, consistent with the fact that the Pc chromodomain binds histone H3 primarily via interactions with residues upstream of H3K27me3 (Min et al., 2003). Nonetheless, we confirmed Ccc1 chromodomain binding to the *C. neoformans* H3K27me2/3 sequence using fluorescence polarization. Chromodomain binding to a fluorescently labeled, human H3K27me3 peptide was competed with increasing amounts of unlabeled *Cryptococcus* H3K27 peptides (Figure 4C). H3K27me2 and me3 peptides compete with apparent affinities of 119 and 28 μM, respectively, while we observed no competition with the unmodified peptide.

To test the importance of the Ccc1 chromodomain in vivo, we generated *ccc1* mutations predicted to disrupt its aromatic cage residues, which mediate methyl-lysine recognition (Eissenberg, 2012). Based on sequence alignment to structurally characterized chromodomains in other systems (Extended Experimental Procedures), two aromatic cage residues in Ccc1 could be identified, which we individually mutated. Strains containing these mutations express Ccc1 at normal levels but show subtelomeric transcript derepression to the same extent as does the *ccc1Δ* strain (Figures 4D and 4E). Using RNA-seq, we observed that the *ccc1-W52A* aromatic cage mutation causes derepression of a set of genes wholly within the set derepressed in *ezh2Δ* cells, whereas the *ccc1Δ* mutant derepresses additional genes (Figure 4F). Thus, the chromodomain mutations appear to separate the Polycomb functions of Ccc1 from its PRC2-independent functions. Consistent with this view, the *ccc1Δ* strain exhibits a growth defect, whereas the *ccc1-W52A* and *ezh2Δ* strains do not (Table S3).

We examined the effect of Ccc1 chromodomain mutations on H3K27me3. ChIP-seq revealed that *ccc1-W52A* cells, like *ccc1Δ* cells, display reduced subtelomeric H3K27me3 domain magnitude and size (13 and 14 kb, respectively, as compared to 41 kb in wild-type) (Figure 4G and Table S1). Furthermore, both the chromodomain mutant and knockout cells show a gain of H3K27me3 at centromeres (Figures 4H and 4I). In the context of the H3K27me3 redistribution in *ccc1-W52A* cells, the total cellular level of this histone mark does not decrease, as assessed by immunoblot (Figure S3B).

These findings demonstrate that the Ccc1 chromodomain recognizes specific histone modifications—H3K27me2/3—and suggest that this activity anchors PRC2 to its product in order to maintain the genome-wide distribution of Polycomb heterochromatin. Consistent with such a role for Ccc1, the *ccc1-W52A* mutation reduces the association of PRC2 with subtelomeric chromatin, as assessed by ChIP of Ezh2 (Figure S3C). At centromeric chromatin, PRC2 association is not detected above background in either wild-type or *ccc1-W52A* cells, indicating that this association is below the limit of detection or that PRC2 is not stably bound to centromeres despite its evident enzymatic action there.

H3K9me2 Heterochromatin Localizes Primarily to Centromeres

Because centromeres are the predominant site of ectopic H3K27me3 in *ccc1* mutants, we hypothesized that PRC2 might be recruited to these improper sites by constitutive heterochromatin, which decorates centromeres in other systems (Grewal and Jia, 2007). To determine the distribution of constitutive heterochromatin in *C. neoformans*, we performed ChIP-seq using an antibody against an associated histone mark: H3K9me2. As expected, wild-type cells exhibit signal primarily at centromeres (Figures 5A and 5C). They also display some H3K9me2 near chromosome ends, but these domains are considerably smaller than those of H3K27me3 (13 kb versus 41 kb) (Figure 5B and Table S1). Quantification of subtelomeric versus centromeric ChIP-seq signal density confirmed this complementary relationship, with H3K9me2 density greatest at centromeres and H3K27me3 greatest at subtelomeres (Figure 5D). Importantly, H3K9me2 signal is eliminated in cells lacking Clr4, the *C. neoformans* ortholog of the H3K9 methyltransferase SUV39H/Su(var)3-9 (Figures 5A–5D). Consistent with a repressive function for H3K9me2, loss of Clr4 results in an approximately 6-fold increase in centromeric transcript levels, as assessed by RNA-seq (Figure S4A).

We next tested whether either type of heterochromatin requires the presence of the other. Cells lacking Ezh2 have no H3K27me3, but exhibit normal H3K9me2, indicating that constitutive heterochromatin does not depend on PRC2 (Figures 5A–5D). Cells lacking Clr4 have no detectable H3K9me2, but exhibit, if anything, a slight increase in total amount of subtelomeric H3K27me3. In addition, these cells contain a total cellular level of H3K27me3 similar to that of wild-type cells, as assessed by immunoblot (Figure S4B). Thus, there is no requirement for Clr4 during the assembly of H3K27me3 domains in otherwise wild-type cells.

(E) Transcript level of Ezh2 target genes in the context of PRC2 subunit mutations, as assessed by RT-qPCR and normalized to 18S rRNA levels. Error bars represent SD.

(F) Venn diagram of genes upregulated >3-fold in *msl1Δ*, *ezh2Δ*, and *ccc1Δ* strains, as determined by RNA-seq.

See also Figure S2 and Tables S2 and S3.

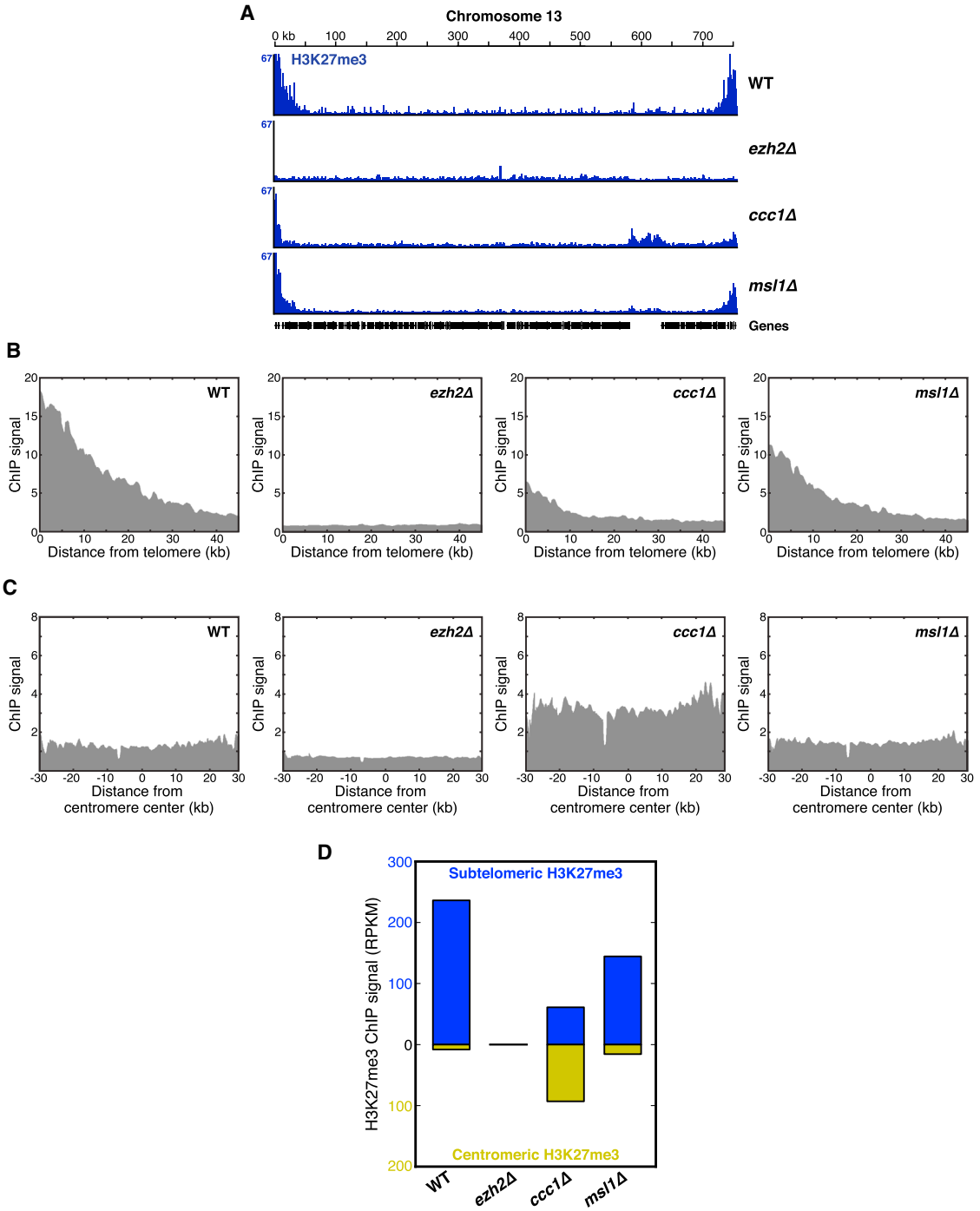

Figure 3. PRC2 Subunits Are Required for the Proper Spatial Deposition of H3K27me3 Heterochromatin

(A) ChIP-seq traces of H3K27me3 signal across chromosome 13 in wild-type cells or cells lacking individual PRC2 components. The gene-poor region near 600 kb corresponds to the centromere.

(B) Average subtelomeric H3K27me3 signal, as measured by ChIP-seq.

(C) Average centromeric H3K27me3 signal, as measured by ChIP-seq.

(D) H3K27me3 at subtelomeric versus centromeric regions, as measured by ChIP-seq. Density (RPKM) of signal above background is reported for subtelomeric regions (blue bar) and centromeric regions (green bar).

H3K9me2 Heterochromatin Directs H3K27me3 Deposition in *ccc1-W52A* Cells

Because the H3K9me2 pattern in wild-type cells coincides with the sites to which H3K27me3 is redistributed in *ccc1* mutants, we tested the hypothesis that the former recruits the latter. First, we used ChIP-seq to measure the genome-wide H3K27me3 distribution in *ccc1-W52A* mutants, *clr4Δ* mutants, and double-mutant cells. As seen before, *ccc1-W52A* mutants show reduced subtelomeric H3K27me3 signal and an emergence of ectopic signal in centromeres (Figures 6A–6D). Remarkably, the loss of Clr4 in the context of *ccc1-W52A* causes a complete loss of centromeric H3K27me3 signal (Figures 6A–6D). Thus, the ectopic redistribution of H3K27me3 in the context of *ccc1-W52A* requires Clr4, which itself deposits H3K9me2. Similarly, the subtelomeric H3K27me3 signal, which is not Clr4-dependent in a wild-type background, becomes Clr4-dependent in the context of *ccc1-W52A* (Figures 6B, 6D, and S5). ChIP-qPCR validation confirms that centromeric and telomeric H3K27me3 is, in the context of *ccc1-W52A*, dependent on H3K9me2 (Figures 6E and S6A). These results suggest that, when the Ccc1 chromodomain is disrupted, H3K9me2 guides the genome-wide deposition of H3K27me3. In further support of this conclusion, the average size of subtelomeric H3K27me3 domains is distinct from that of H3K9me2 domains in wild-type cells (41 kb for H3K27me3 versus 13 kb for H3K9me2) but becomes similar in the context of *ccc1-W52A* (13 kb versus 9 kb), consistent with a collapse of H3K27me3 onto sites of H3K9me2 when Ccc1 is mutated (Table S1).

We considered what features of PRC2 might enable it to respond to signals that emanate from constitutive heterochromatin. In higher eukaryotes, the EED/Esc WD40 domains contain a pocket that can bind methyl-lysine side chains (Margueron et al., 2009; Xu et al., 2010). This interaction stimulates the methyltransferase activity of EZH2/E(z) and is required for recruitment of PRC2 to its target loci (Margueron et al., 2009). However, the pocket in EED/Esc is not specific for H3K27me3: it can bind several different histone tail methyl-lysine residues, with silenced gene marks (such as H3K27me3 and H3K9me3) tending to bind EED/Esc with higher affinity and to activate PRC2 more strongly than do active gene marks (such as H3K4me3 and H3K36me3) (Margueron et al., 2009; Xu et al., 2010). These findings suggested the possibility that the yeast Eed1 might promote ectopic H3K27me3 in the *ccc1-W52A* mutant.

To test this hypothesis, we first recombinantly expressed full-length *C. neoformans* Eed1 in *E. coli* and tested its ability to bind histone tail peptides using an in-solution peptide pull-down assay. GST-Eed1 interacts with peptides corresponding to the first 20 residues of histone H3, with a modest (but consistent) preference for the repressive marks H3K9me1/2/3 (Figure S6B). In contrast, the activation-associated marks H3K4me3 and polyacetylated H3 cause, respectively, a reduction or elimination of Eed1 binding, further consistent with the idea that Eed1 prefers an H3K9me heterochromatin signature (Figure S6B). Next, we generated a *C. neoformans* strains in which a conserved tyrosine residue in the putative Eed1 methyl-lysine binding pocket is mutated. We observed that this single amino acid replacement of Eed1, which is expressed at normal levels in cells, significantly reduces the ectopic, Clr4-dependent H3K27me3 induced by Ccc1-W52A (Figures S6C and S6D). The Eed1-Y134A mutation has a significantly weaker effect on the eutopic, Clr4-independent H3K27me3 observed at subtelomeric regions in otherwise wild-type cells harboring a functional Ccc1 protein (Figure S6E). Thus, direct sensing of H3K9me2 and other histone marks by Eed1 may be in part responsible for the aberrant H3K27 trimethylation in Ccc1 chromodomain mutants.

DISCUSSION

The Polycomb system is central to animal and plant development and plays a key role in human disease. Despite the importance of these chromatin regulators, how they guide the establishment and inheritance of repressive H3K27me domains remains poorly understood. In this paper, we describe the Polycomb system of a budding yeast, *C. neoformans*. We identify a PRC2-like complex that mediates all genome-wide H3K27me3 via its catalytic Ezh2 subunit. Our genetic and biochemical dissection of the other PRC2 components reveals distinct roles for different subunits. Most strikingly, our results demonstrate that product recognition by a chromodomain subunit masks a latent promiscuity of PRC2 by which it is attracted to centromeric H3K9me2 domains, where H3K27me3 is not normally deposited. As chromatin-modifying enzymes typically contain product recognition modules, these findings have general implications.

H3K27me3 and PRC2 in a Budding Yeast

In contrast to *S. cerevisiae* and *S. pombe*, the human fungal pathogen *C. neoformans* encodes an ortholog not only of the H3K9 methyltransferase Clr4 but also of the H3K27 methyltransferase EZH2/E(z). By generating modification-specific antibodies, we found that H3K27me3 is deposited by the EZH2/E(z) ortholog across subtelomeric domains that repress the expression of underlying genes and noncoding transcripts. Polycomb heterochromatin may therefore have a specialized role in the regulation of subtelomeres, which in fungi are enriched for rapidly-evolving genes involved in niche adaptation and specialized metabolic functions (Brown et al., 2010; Chow et al., 2012). Consistent with this idea, the 41 kb average size of subtelomeric H3K27me3 domains closely matches a computational prediction of *C. neoformans* subtelomere size based on enrichment for metabolism-related gene products (~40 kb) (Chow et al., 2012). Intriguingly, subtelomeric genes in other pathogenic fungi are silenced by domains of repressive chromatin and respond to environmental changes during the process of host infection, raising the possibility that Polycomb heterochromatin could contribute to the pathogenicity of *C. neoformans* (Domergue et al., 2005; De Las Peñas et al., 2003; McDonagh et al., 2008).

We found that H3K9me2 domains also repress transcript levels, but are deposited at largely spatially distinct locations, analogous to the distinct patterns of these two chromatin types in metazoans (Filion et al., 2010; Kharchenko et al., 2011; Rosenfeld et al., 2009). H3K9me2 domains are found primarily at centromeres, consistent with their broadly conserved roles in centromere function and chromosome segregation (Grewal and Jia, 2007). We also observed small regions of H3K9me2 deposition at subtelomeres. These are approximately 25% the size of the H3K27me3 domains with which they overlap. Both

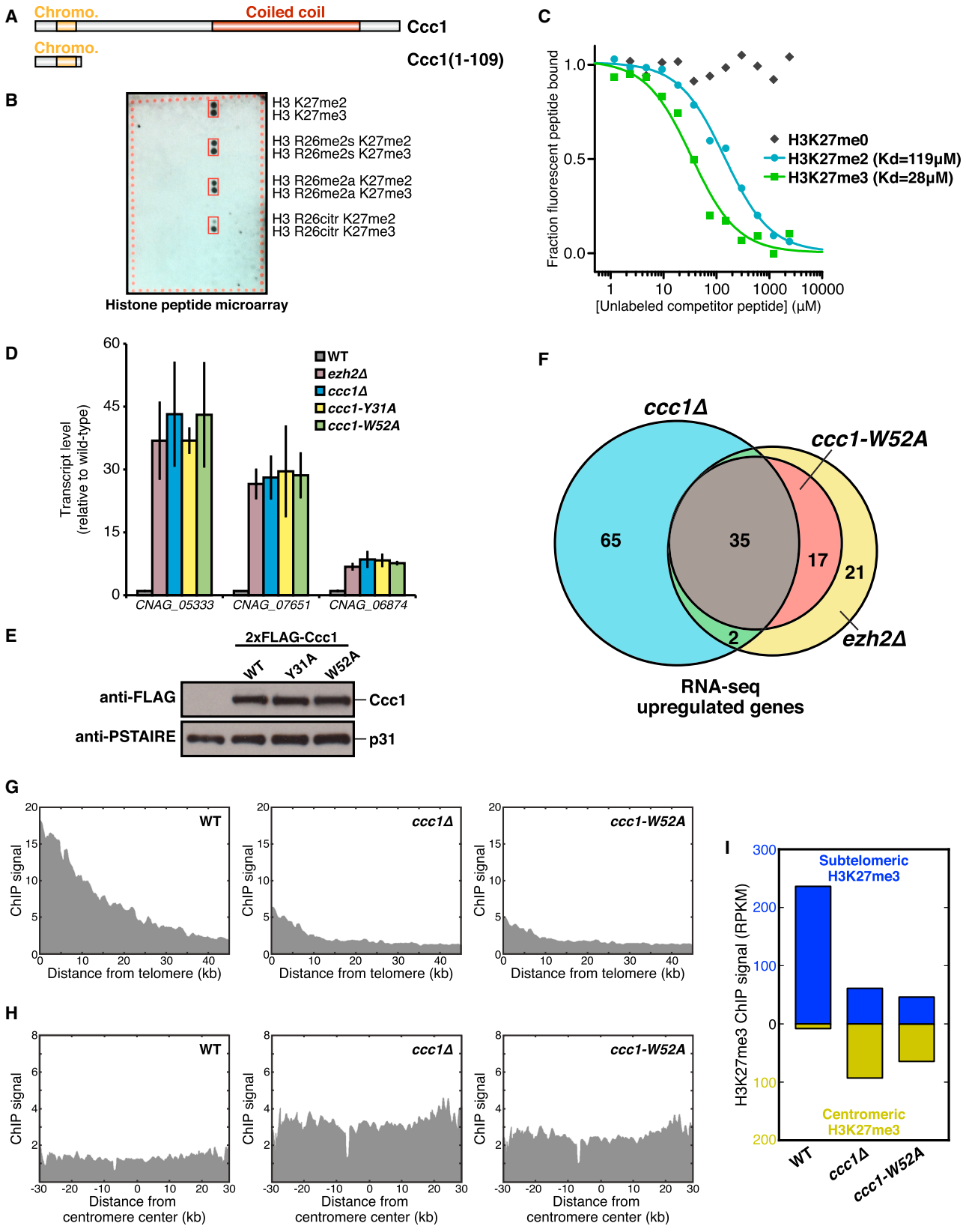

(legend on next page)

the H3K27me3 and H3K9me2 domains exhibit a distinctive shape: their ChIP enrichments are greatest at the chromosome termini, and taper off toward the chromosome interior. The spread of the two types of marks is evidently mutually independent, because neither chromatin mark depends on the other for its proper distribution.

In higher eukaryotes, EZH2/E(z) activity is extensively regulated by its protein interaction partners within PRC2 (O'Meara and Simon, 2012). Our biochemical purifications of PRC2/E(z) protein orthologs in *Cryptococcus* suggest the existence of a PRC2-like core complex of at least five components, all of which functionally contribute to the formation of H3K27me3 domains of the proper size and location. Three of these components—Ezh2, Eed1, and Msl1—are clear orthologs of mammalian PRC2 components, whereas two others—Bnd1 and Ccc1—appear to be fungal-specific proteins, although they may have functions analogous to those of other mammalian PRC2 and/or PRC1 components.

We identified additional chromatin-related proteins in purifications of particular PRC2 components. Among these is a class II histone deacetylase homolog, Clr3, whose removal caused subtelomeric gene derepression. Analogously, the mammalian NuRD complex, which contains a Clr3-related histone deacetylase, has recently been shown to facilitate PRC2 recruitment in embryonic stem cells (Reynolds et al., 2012).

Product Recognition Suppresses Latent Promiscuity of the PRC2 Complex

One subunit of the *C. neoformans* PRC2 complex, Ccc1, harbors a chromodomain, a protein motif that typically binds to histone tails in a manner dependent on methylation of a specific lysine residue. Indeed, our biochemical studies demonstrated that this domain binds PRC2 reaction products—H3K27me2/3—but not other histone tail modifications. Remarkably, mutation of the Ccc1 chromodomain at residues responsible for methyl-lysine recognition causes a genome-wide redistribution of H3K27me3: the subtelomeric H3K27me3 domains shrink in size and ectopic H3K27me3 domains arise at centromeres. Strikingly, this altered H3K27me3 distribution coincides with the genomic sites of H3K9me2 heterochromatin. This observation led us to hypothesize that the Ccc1 chromodomain suppresses a latent attraction of PRC2 to signals from H3K9me2 heterochromatin. Indeed, we found that the ectopic deposition of H3K27me3 at centromeres in the context of Ccc1 chromodomain disruption is completely suppressed by removal of the H3K9 methyltransferase Clr4. These findings demonstrate a role for product recognition in ensuring the fidelity of a chromatin-modifying complex by suppressing the influence of inappropriate signals (Figure 7).

Although we suspect that multiple features make heterochromatin attractive to PRC2, our analysis of a conserved tyrosine residue in Eed1 predicted to be involved in methyl-lysine binding suggests that H3K9me2 may be one such inappropriate signal (Margueron et al., 2009; Xu et al., 2010). Further detailed mechanistic tests of this model will require reconstitution of an active *C. neoformans* complex in vitro. In human EED, methyl-lysine binding specificity is remarkably broad (Margueron et al., 2009), raising the possibility that PRC2 complexes may be generally susceptible to aberrant recruitment. Additional inputs are known to impact PRC2, which include histone modifications, chromatin density, noncoding RNA, and posttranslational modification of EZH2/E(z) itself (O'Meara and Simon, 2012). As many of these features are found in H3K9me-marked heterochromatin, they likely also serve as latent "attractants" for PRC2. Because removal of Clr4 does not reduce H3K27me3 in otherwise wild-type cells (but reduces H3K27me3 in *ccc1* mutant cells), an important additional conclusion is that product recognition by Ccc1 is required not only to shield PRC2 from inappropriate signals but also for the assembly of H3K27me3 domains per se, perhaps by facilitating spread of the H3K27me3 mark.

H3K27me-specific chromodomains in other eukaryotes may also act to promote the fidelity of chromatin transactions. In higher eukaryotes, Polycomb repressive complex 1 (PRC1) includes the eponymous Polycomb protein, which contains an H3K27me-specific chromodomain that is thought in some settings to guide the complex to sites where PRC2 has been active, thereby positioning PRC1 to repress transcription (Sparmann and van Lohuizen, 2006). The ability of PRC1 and PRC2 components to physically interact raises the possibility that PRC1 might also provide product recognition activity for PRC2, analogous to the role of Ccc1 (Cao et al., 2014; Poux et al., 2001). However, intriguing recent work on animal Polycomb systems raises additional possibilities. In particular, several studies have demonstrated that a modification catalyzed by PRC1—H2A monoubiquitylation (H2AUb)—can recruit PRC2 in vivo, changing the view that PRC2 acts strictly upstream of PRC1

Figure 4. The Ccc1 Chromodomain Binds H3K27me2/3 and Is Required for Proper Spatial Positioning of H3K27me3 Heterochromatin

(A) Predicted domains of full-length Ccc1 and of the truncated construct Ccc1(1-109) that was expressed recombinantly.

(B) Binding of Ccc1 chromodomain to a modified histone peptide array, detected by chemiluminescence using an anti-GST antibody. The eight bound peptides are labeled at right.

(C) Binding of Ccc1 chromodomain to methylated or unmethylated H3K27 peptides, as assessed by fluorescence polarization binding assay. Ccc1(1-109) was bound to a fluorescently-labeled H3K27me3 peptide, and this labeled peptide was competed off with increasing concentrations of unlabeled *C. neoformans* H3K27me0/2/3.

(D) Transcript level of Ezh2 target genes in the context of Ccc1 chromodomain mutations, as assessed by RT-qPCR and normalized to 18S rRNA levels. Error bars represent SD.

(E) Expression level of Ccc1 chromodomain mutants, as assessed by immunoblot using the antibodies indicated at left. p31 serves as a loading control.

(F) Venn diagram of genes upregulated >3-fold in *ccc1Δ, ccc1-W52A,* and *ezh2Δ* strains, as determined by RNA-seq.

(G) Average subtelomeric H3K27me3 signal, as measured by ChIP-seq.

(H) Average centromeric H3K27me3 signal, as measured by ChIP-seq.

(I) H3K27me3 at subtelomeric versus centromeric regions, as measured by ChIP-seq.

See also Figure S3.

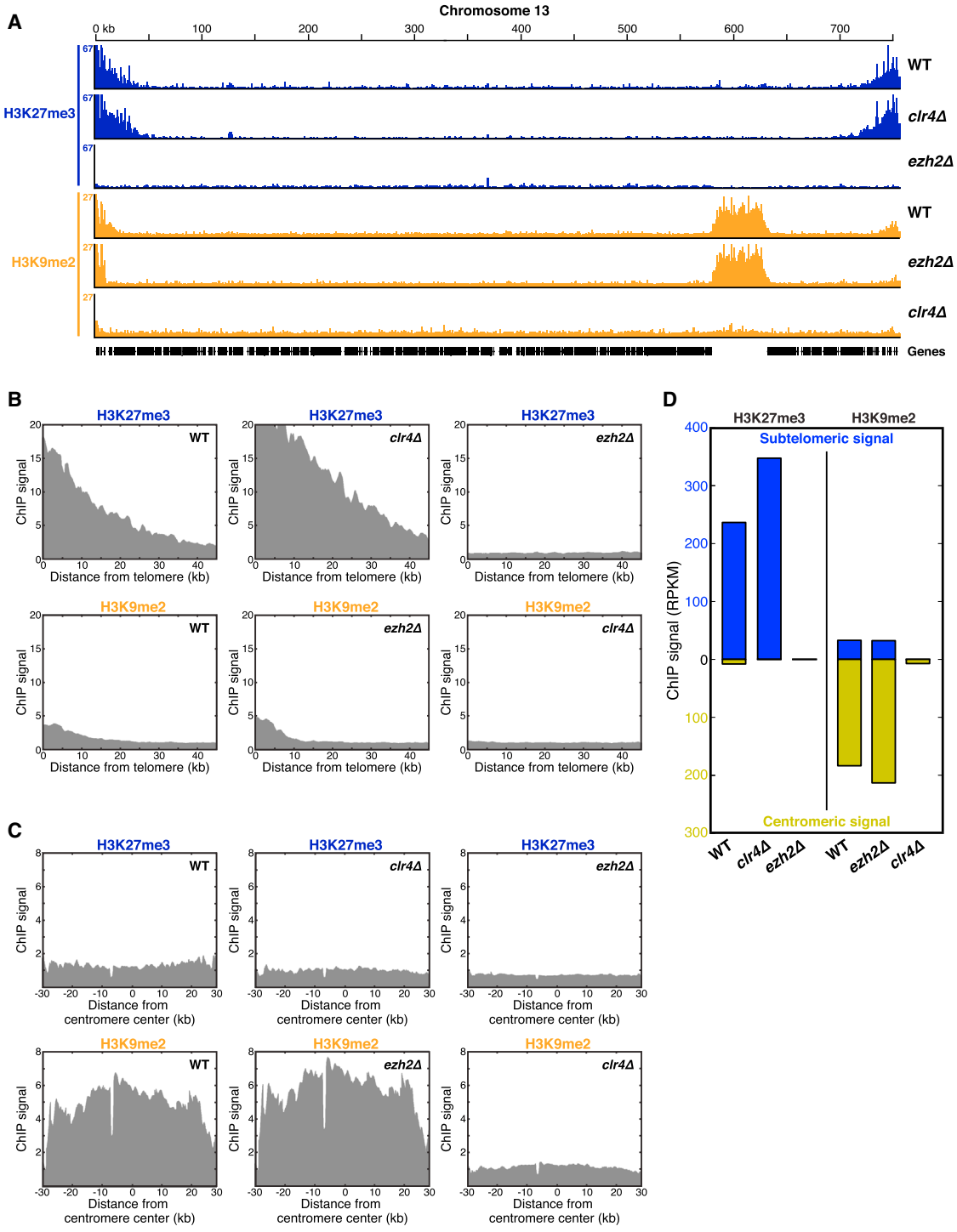

Figure 5. H3K9me2 Heterochromatin Decorates Centromeres and Small Subtelomeric Regions in *C. neoformans*

(A) ChIP-seq traces of H3K27me3 signal (blue) and H3K9me2 signal (orange) across chromosome 13 in wild-type cells or cells lacking Clr4 or Ezh2, the methyltransferases for H3K9 and H3K27, respectively.

(B) Average subtelomeric H3K27me3 and H3K9me2 signal, as measured by ChIP-seq.

(C) Average centromeric H3K27me3 and H3K9me2 signal, as measured by ChIP-seq.

(D) H3K27me3 and H3K9me2 at subtelomeric versus centromeric regions, as measured by ChIP-seq.

See also Figure S4.

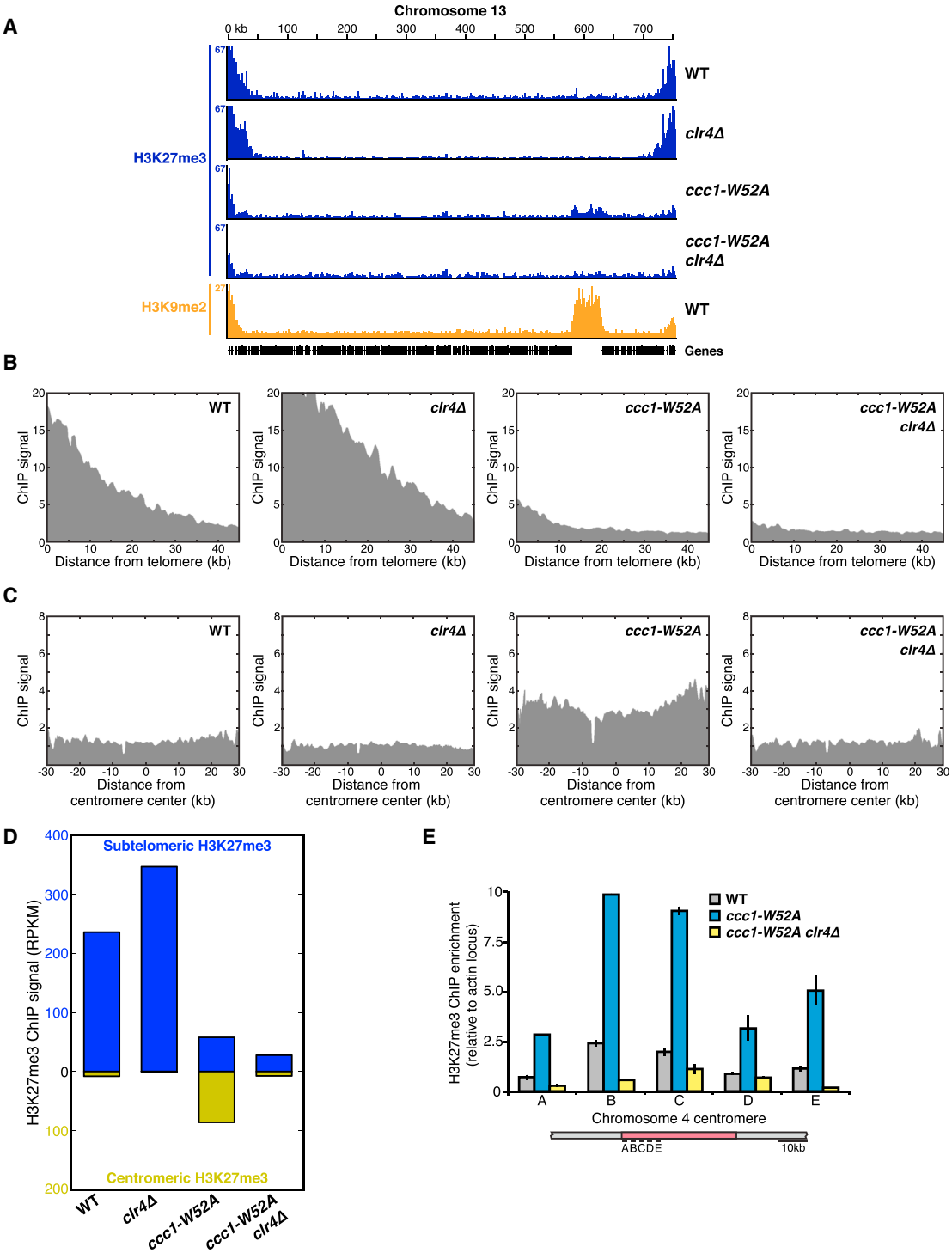

Figure 6. Constitutive Heterochromatin Instructs H3K27me3 in the *ccc1-W52A* Mutant

(A) ChIP-seq traces of H3K27me3 signal (blue) and H3K9me2 signal (orange) across chromosome 13.

(B) Average subtelomeric H3K27me3 signal, as measured by ChIP-seq.

(C) Average centromeric H3K27me3 signal, as measured by ChIP-seq.

(D) H3K27me3 at subtelomeric versus centromeric regions, as measured by ChIP-seq.

(E) H3K27me3 enrichment at five centromeric loci (below) in the context of Ccc1 chromodomain mutations, as assessed by ChIP-qPCR. Signal was normalized to WCE and plotted relative to signal at the euchromatic actin locus. Error bars represent SD.

See also Figures S5 and S6.

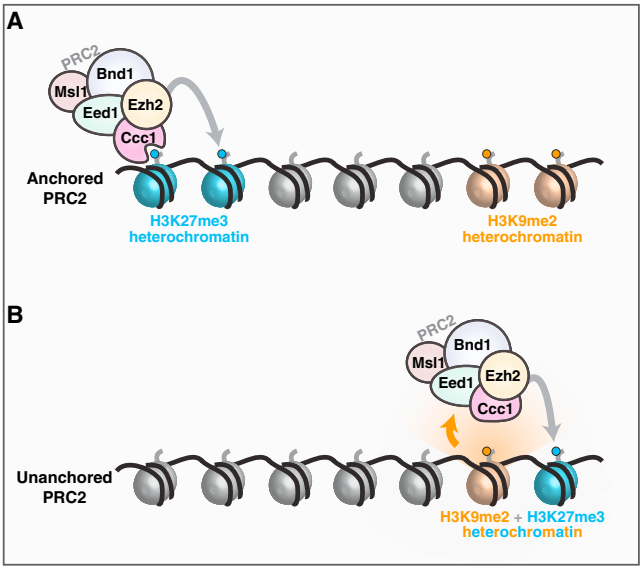

Figure 7. Model for the Role of Product Recognition by *C. neoformans* PRC2

(A) In wild-type cells, PRC2 deposits repressive H3K27me3 at subtelomeres. The Ccc1 subunit of PRC2 binds H3K27me3 via its chromodomain, thereby anchoring PRC2 to its product. In this context, subtelomeric H3K27me3 does not depend on the presence of H3K9me2, and these two chromatin types are largely distinct in location.

(B) In the context of the *ccc1-W52A* mutant, PRC2 lacks product recognition activity and is not anchored to H3K27me3 by Ccc1. In this setting, H3K27me3 is redistributed to sites of H3K9me2, including centromeres, and this redistribution depends on the presence of Clr4. Thus, unanchored PRC2 inappropriately responds to signals from another chromatin type, H3K9me2 heterochromatin, which causes ectopic redistribution of H3K27me3. These signals may include direct H3K9me2 binding by Eed1 (orange arrow) as well as recognition of the other features of heterochromatin such as its nucleosome density and its specific patterns of additional histone modifications (orange ray).

(Blackledge et al., 2014; Cooper et al., 2014). In this scenario, PRC2 would not directly recognize its own product, but would rather bind a modification deposited by an enzyme, PRC1, that itself had previously been recruited by the PRC2 product. Such a mechanism could have a functional impact equivalent to that described here: the tethering of PRC2 to the sites of its product. A situation more directly analogous to the yeast system may occur in plants, where a chromodomain protein called LHP1 binds to both the RbAp46/48/Nurf55 ortholog as well as to H3K27me2/3, thereby linking PRC2 to its product (Derkacheva et al., 2013). Assessing the potential role of product recognition in the fidelity of animal and plant Polycomb systems will require generation of specific mutations that disrupt product recognition (be it H3K27me or H2AUb) and assessment of their impact on the fidelity of chromatin modification via genome-wide ChIP studies.

Given our results, it is notable that there are some hints in higher eukaryotes that Polycomb systems may interact with constitutive heterochromatin, both in normal or pathologic contexts. For example, although H3K27me and H3K9me repressive chromatin domains are generally separated in these organisms, overlap at a subset of targets has been observed in some cell types (Bilodeau et al., 2009; Mozzetta et al., 2014; Wang et al., 2008), suggesting potential functional interaction. Such interactions may contribute to pathology as well: coincident H3K27me and H3K9me deposition at the INK4/ARF locus, a key tumor suppressor, is associated with spontaneous transformation of mesenchymal stem cells, raising the possibility that the reconfiguration of H3K27me patterns could be oncogenic (Zheng et al., 2013).

In contrast to many other enzyme classes, chromatin-modifying complexes typically harbor product recognition modules, either encoded within the same polypeptide as the enzymatic domain or on an associated protein. This attribute can be important for the local spread of a modification and has been hypothesized to assist in positive feedback as well as epigenetic inheritance of chromatin states across cell division (Collins et al., 2008; Hansen et al., 2008; Hassan et al., 2002; Klein et al., 2014; Lan et al., 2007; Liou et al., 2005; Margueron et al., 2009; Zhang et al., 2008; Zhu and Reinberg, 2011). Our findings demonstrate a conceptually distinct (but not mutually exclusive) role for product recognition: to anchor a chromatin-modifying complex to its target, thereby preventing its aberrant recruitment by signals from a distinct type of chromatin. Because nucleosomes exist at high copy-number, with a concentration of ~0.1 mM in mammalian interphase nuclei (Hihara et al., 2012), chromatin-modifying complexes likely operate in an environment that is rich in off-target substrates. Thus, fidelity-enhancing mechanisms of the type described here are likely to be an important, underexplored aspect of chromatin-based genome regulation.

EXPERIMENTAL PROCEDURES

Yeast Strains

Yeast strains used in this study are listed in Table S4. All *C. neoformans* strains were derived from strain H99 using published procedures (Chun and Madhani, 2010).

Tandem Affinity Protein Purification

C. neoformans strains encoding CBP-2xFLAG-tagged proteins expressed from their endogenous promoters were grown to log phase, harvested, and snap frozen. Frozen cells were lysed in a coffee grinder and tagged proteins were purified using anti-FLAG M2 (Sigma) resin, after which they were eluted using 3xFLAG peptide (Sigma). A second purification step was performed using calmodulin resin (Stratagene), after which the bound protein was eluted using 3 mM EGTA and analyzed by zinc stain (Pierce) or mass spectrometry as described in Table S5 and elsewhere (Dumesic et al., 2013).

RNA Isolation and Expression Profiling

Total RNA was isolated using TRIzol (Invitrogen). For RT-qPCR, RNA was treated with DNaseI (Roche) and then Superscript III (Invitrogen) to generate cDNA. PCR primers are listed in Table S6. For RNA-seq, mRNA was isolated from total RNA using the Oligotex mRNA mini kit (QIAGEN) and two biological replicate sequencing libraries were prepared for each genotype using the NEBNext Ultra Directional RNA Library Prep Kit (New England Biolabs) as described in Extended Experimental Procedures.

Chromatin Immunoprecipitation

C. neoformans cultures were crosslinked with formaldehyde and lysate was generated using a Mini-Beadbeater (Biospec Products), from which DNA was isolated and sheared in a Bioruptor waterbath sonicator (Diagenode). Antibodies against H3K27me3 (generated in this study) and H3K9me2 (ab1220, Abcam) were used for immunoprecipitation. The resulting DNA was analyzed by qPCR using primers listed in Table S6 or by high throughput

sequencing (1–3 replicates per genotype) as described in Extended Experimental Procedures. Meta-telomeres (or meta-centromeres) were generated by aligning all such regions in the genome, calculating average sequencing read coverage, and normalizing both to a WCE sample as well as for differences in total read count between samples.

Recombinant Protein Expression and Binding Assays

Codon-optimized vectors were expressed in *E. coli*. Purified GST-tagged Ccc1 chromodomain was bound to a MODified histone peptide array (Active Motif) and detected by chemiluminescence using anti-GST antibodies. To measure dissociation constants, the binding of recombinant Ccc1 chromodomain to a fluorescent H3K27me3 peptide was competed using increasing concentrations of unlabeled H3K27me0/2/3 peptide, with binding measured by fluorescence polarization.

ACCESSION NUMBERS

ChIP-seq and RNA-seq data were deposited in the Gene Expression Omnibus under accession number GSE61550.

SUPPLEMENTAL INFORMATION

Supplemental Information includes Extended Experimental Procedures, six figures, and eight tables and can be found with this article online at http://dx.doi.org/10.1016/j.cell.2014.11.039.

AUTHOR CONTRIBUTIONS

P.A.D. and H.D.M. designed the study. P.A.D. performed experiments shown in Figures 1, 2, 3, 4, 5, 6, S1, S2, S3, S4, S5, and S6. C.M.H. performed bioinformatic analyses in Figures 1, 2, 3, 4, 5, 6, S1, S4, and S5. J.J.M. and J.R.Y. performed mass spectrometry analyses shown in Figure 2. L.R.P and D.G.F. provided protocols and reagents for peptide binding assays shown in Figure 4. E.K.S. and B.D.S. performed recombinant protein expression and pull-down assay shown in Figure S6B and provided protocols and advice for antibody production. S.M.C. provided protocols and assistance in recombinant protein expression. P.A.D. and H.D.M. wrote the manuscript. All authors contributed to editing the manuscript.

ACKNOWLEDGMENTS

We thank members of the Madhani lab for helpful discussions, N. Nguyen for media preparation, Krzysztof Krajewski and the University of North Carolina High-Throughput Peptide Synthesis and Arraying Facility for histone peptide production, and Geeta Narlikar for critical reading of the manuscript. Mass spectrometry experiments were supported by the National Center for Research Resources (5P41RR011823-17), the National Institute of General Medical Sciences (8 P41 GM103533-17), and the National Institute on Aging (R01AG027463-04).

Received: July 3, 2014
Revised: September 30, 2014
Accepted: November 12, 2014
Published: December 18, 2014

REFERENCES

Aloia, L., Di Stefano, B., and Di Croce, L. (2013). Polycomb complexes in stem cells and embryonic development. Development *140*, 2525–2534.

Bender, S., Tang, Y., Lindroth, A.M., Hovestadt, V., Jones, D.T.W., Kool, M., Zapatka, M., Northcott, P.A., Sturm, D., Wang, W., et al. (2013). Reduced H3K27me3 and DNA hypomethylation are major drivers of gene expression in K27M mutant pediatric high-grade gliomas. Cancer Cell *24*, 660–672.

Bilodeau, S., Kagey, M.H., Frampton, G.M., Rahl, P.B., and Young, R.A. (2009). SetDB1 contributes to repression of genes encoding developmental regulators and maintenance of ES cell state. Genes Dev. *23*, 2484–2489.

Blackledge, N.P., Farcas, A.M., Kondo, T., King, H.W., McGouran, J.F., Hanssen, L.L.P., Ito, S., Cooper, S., Kondo, K., Koseki, Y., et al. (2014). Variant PRC1 complex-dependent H2A ubiquitylation drives PRC2 recruitment and polycomb domain formation. Cell *157*, 1445–1459.

Brown, C.A., Murray, A.W., and Verstrepen, K.J. (2010). Rapid expansion and functional divergence of subtelomeric gene families in yeasts. Curr. Biol. *20*, 895–903.

Cao, Q., Wang, X., Zhao, M., Yang, R., Malik, R., Qiao, Y., Poliakov, A., Yocum, A.K., Li, Y., Chen, W., et al. (2014). The central role of EED in the orchestration of polycomb group complexes. Nat Commun *5*, 3127.

Chalker, D.L., Meyer, E., and Mochizuki, K. (2013). Epigenetics of ciliates. Cold Spring Harb. Perspect. Biol. *5*, a017764–a017764.

Chow, E.W.L., Morrow, C.A., Djordjevic, J.T., Wood, I.A., and Fraser, J.A. (2012). Microevolution of Cryptococcus neoformans driven by massive tandem gene amplification. Mol. Biol. Evol. *29*, 1987–2000.

Chun, C.D., and Madhani, H.D. (2010). Applying genetics and molecular biology to the study of the human pathogen Cryptococcus neoformans. Methods Enzymol. *470*, 797–831.

Collins, R.E., Northrop, J.P., Horton, J.R., Lee, D.Y., Zhang, X., Stallcup, M.R., and Cheng, X. (2008). The ankyrin repeats of G9a and GLP histone methyltransferases are mono- and dimethyllysine binding modules. Nat. Struct. Mol. Biol. *15*, 245–250.

Connolly, L.R., Smith, K.M., and Freitag, M. (2013). The Fusarium graminearum histone H3 K27 methyltransferase KMT6 regulates development and expression of secondary metabolite gene clusters. PLoS Genet. *9*, e1003916.

Cooper, S., Dienstbier, M., Hassan, R., Schermelleh, L., Sharif, J., Blackledge, N.P., De Marco, V., Elderkin, S., Koseki, H., Klose, R., et al. (2014). Targeting polycomb to pericentric heterochromatin in embryonic stem cells reveals a role for H2AK119u1 in PRC2 recruitment. Cell Rep *7*, 1456–1470.

De Las Peñas, A., Pan, S.J., Castaño, I., Alder, J., Cregg, R., and Cormack, B.P. (2003). Virulence-related surface glycoproteins in the yeast pathogen Candida glabrata are encoded in subtelomeric clusters and subject to RAP1- and SIR-dependent transcriptional silencing. Genes Dev. *17*, 2245–2258.

Derkacheva, M., Steinbach, Y., Wildhaber, T., Mozgová, I., Mahrez, W., Nanni, P., Bischof, S., Gruissem, W., and Hennig, L. (2013). Arabidopsis MSI1 connects LHP1 to PRC2 complexes. EMBO J. *32*, 2073–2085.

Domergue, R., Castaño, I., De Las Peñas, A., Zupancic, M., Lockatell, V., Hebel, J.R., Johnson, D., and Cormack, B.P. (2005). Nicotinic acid limitation regulates silencing of Candida adhesins during UTI. Science *308*, 866–870.

Dumesic, P.A., Natarajan, P., Chen, C., Drinnenberg, I.A., Schiller, B.J., Thompson, J., Moresco, J.J., Yates, J.R., 3rd, Bartel, D.P., and Madhani, H.D. (2013). Stalled spliceosomes are a signal for RNAi-mediated genome defense. Cell *152*, 957–968.

Eissenberg, J.C. (2012). Structural biology of the chromodomain: form and function. Gene *496*, 69–78.

Filion, G.J., van Bemmel, J.G., Braunschweig, U., Talhout, W., Kind, J., Ward, L.D., Brugman, W., de Castro, I.J., Kerkhoven, R.M., Bussemaker, H.J., and van Steensel, B. (2010). Systematic protein location mapping reveals five principal chromatin types in Drosophila cells. Cell *143*, 212–224.

Grewal, S.I.S., and Jia, S. (2007). Heterochromatin revisited. Nat. Rev. Genet. *8*, 35–46.

Hansen, K.H., Bracken, A.P., Pasini, D., Dietrich, N., Gehani, S.S., Monrad, A., Rappsilber, J., Lerdrup, M., and Helin, K. (2008). A model for transmission of the H3K27me3 epigenetic mark. Nat. Cell Biol. *10*, 1291–1300.

Hassan, A.H., Prochasson, P., Neely, K.E., Galasinski, S.C., Chandy, M., Carrozza, M.J., and Workman, J.L. (2002). Function and selectivity of bromodomains in anchoring chromatin-modifying complexes to promoter nucleosomes. Cell *111*, 369–379.

Hihara, S., Pack, C.-G., Kaizu, K., Tani, T., Hanafusa, T., Nozaki, T., Takemoto, S., Yoshimi, T., Yokota, H., Imamoto, N., et al. (2012). Local nucleosome dynamics facilitate chromatin accessibility in living mammalian cells. Cell Rep *2*, 1645–1656.

Jamieson, K., Rountree, M.R., Lewis, Z.A., Stajich, J.E., and Selker, E.U. (2013). Regional control of histone H3 lysine 27 methylation in Neurospora. Proc. Natl. Acad. Sci. USA *110*, 6027–6032.

Janbon, G., Ormerod, K.L., Paulet, D., Byrnes, E.J., 3rd, Yadav, V., Chatterjee, G., Mullapudi, N., Hon, C.-C., Billmyre, R.B., Brunel, F., et al. (2014). Analysis of the genome and transcriptome of Cryptococcus neoformans var. grubii reveals complex RNA expression and microevolution leading to virulence attenuation. PLoS Genet. *10*, e1004261.

Kharchenko, P.V., Alekseyenko, A.A., Schwartz, Y.B., Minoda, A., Riddle, N.C., Ernst, J., Sabo, P.J., Larschan, E., Gorchakov, A.A., Gu, T., et al. (2011). Comprehensive analysis of the chromatin landscape in Drosophila melanogaster. Nature *471*, 480–485.

Klein, B.J., Piao, L., Xi, Y., Rincon-Arano, H., Rothbart, S.B., Peng, D., Wen, H., Larson, C., Zhang, X., Zheng, X., et al. (2014). The histone-H3K4-specific demethylase KDM5B binds to its substrate and product through distinct PHD fingers. Cell Rep. *6*, 325–335.

Klose, R.J., Cooper, S., Farcas, A.M., Blackledge, N.P., and Brockdorff, N. (2013). Chromatin sampling—an emerging perspective on targeting polycomb repressor proteins. PLoS Genet. *9*, e1003717.

Lan, F., Collins, R.E., De Cegli, R., Alpatov, R., Horton, J.R., Shi, X., Gozani, O., Cheng, X., and Shi, Y. (2007). Recognition of unmethylated histone H3 lysine 4 links BHC80 to LSD1-mediated gene repression. Nature *448*, 718–722.

Liou, G.-G., Tanny, J.C., Kruger, R.G., Walz, T., and Moazed, D. (2005). Assembly of the SIR complex and its regulation by O-acetyl-ADP-ribose, a product of NAD-dependent histone deacetylation. Cell *121*, 515–527.

Liu, Y., Taverna, S.D., Muratore, T.L., Shabanowitz, J., Hunt, D.F., and Allis, C.D. (2007). RNAi-dependent H3K27 methylation is required for heterochromatin formation and DNA elimination in Tetrahymena. Genes Dev. *21*, 1530–1545.

Margueron, R., and Reinberg, D. (2011). The Polycomb complex PRC2 and its mark in life. Nature *469*, 343–349.

Margueron, R., Justin, N., Ohno, K., Sharpe, M.L., Son, J., Drury, W.J., 3rd, Voigt, P., Martin, S.R., Taylor, W.R., De Marco, V., et al. (2009). Role of the polycomb protein EED in the propagation of repressive histone marks. Nature *461*, 762–767.

McDonagh, A., Fedorova, N.D., Crabtree, J., Yu, Y., Kim, S., Chen, D., Loss, O., Cairns, T., Goldman, G., Armstrong-James, D., et al. (2008). Sub-telomere directed gene expression during initiation of invasive aspergillosis. PLoS Pathog. *4*, e1000154.

Min, J., Zhang, Y., and Xu, R.-M. (2003). Structural basis for specific binding of Polycomb chromodomain to histone H3 methylated at Lys 27. Genes Dev. *17*, 1823–1828.

Mozzetta, C., Pontis, J., Fritsch, L., Robin, P., Portoso, M., Proux, C., Margueron, R., and Ait-Si-Ali, S. (2014). The histone H3 lysine 9 methyltransferases G9a and GLP regulate polycomb repressive complex 2-mediated gene silencing. Mol. Cell *53*, 277–289.

O'Meara, M.M., and Simon, J.A. (2012). Inner workings and regulatory inputs that control Polycomb repressive complex 2. Chromosoma *121*, 221–234.

Plass, C., Pfister, S.M., Lindroth, A.M., Bogatyrova, O., Claus, R., and Lichter, P. (2013). Mutations in regulators of the epigenome and their connections to global chromatin patterns in cancer. Nat. Rev. Genet. *14*, 765–780.

Popovic, R., Martinez-Garcia, E., Giannopoulou, E.G., Zhang, Q., Zhang, Q., Ezponda, T., Shah, M.Y., Zheng, Y., Will, C.M., Small, E.C., et al. (2014). Histone methyltransferase MMSET/NSD2 alters EZH2 binding and reprograms the myeloma epigenome through global and focal changes in H3K36 and H3K27 methylation. PLoS Genet. *10*, e1004566.

Poux, S., Melfi, R., and Pirrotta, V. (2001). Establishment of Polycomb silencing requires a transient interaction between PC and ESC. Genes Dev. *15*, 2509–2514.

Reynolds, N., Salmon-Divon, M., Dvinge, H., Hynes-Allen, A., Balasooriya, G., Leaford, D., Behrens, A., Bertone, P., and Hendrich, B. (2012). NuRD-mediated deacetylation of H3K27 facilitates recruitment of Polycomb Repressive Complex 2 to direct gene repression. EMBO J. *31*, 593–605.

Rosenfeld, J.A., Wang, Z., Schones, D.E., Zhao, K., DeSalle, R., and Zhang, M.Q. (2009). Determination of enriched histone modifications in non-genic portions of the human genome. BMC Genomics *10*, 143.

Shaver, S., Casas-Mollano, J.A., Cerny, R.L., and Cerutti, H. (2010). Origin of the polycomb repressive complex 2 and gene silencing by an E(z) homolog in the unicellular alga Chlamydomonas. Epigenetics *5*, 301–312.

Simon, J.A., and Kingston, R.E. (2009). Mechanisms of polycomb gene silencing: knowns and unknowns. Nat. Rev. Mol. Cell Biol. *10*, 697–708.

Simon, J.A., and Kingston, R.E. (2013). Occupying chromatin: Polycomb mechanisms for getting to genomic targets, stopping transcriptional traffic, and staying put. Mol. Cell *49*, 808–824.

Song, J., Angel, A., Howard, M., and Dean, C. (2012). Vernalization - a cold-induced epigenetic switch. J. Cell Sci. *125*, 3723–3731.

Sparmann, A., and van Lohuizen, M. (2006). Polycomb silencers control cell fate, development and cancer. Nat. Rev. Cancer *6*, 846–856.

Steffen, P.A., and Ringrose, L. (2014). What are memories made of? How Polycomb and Trithorax proteins mediate epigenetic memory. Nat. Rev. Mol. Cell Biol. *15*, 340–356.

Suganuma, T., Pattenden, S.G., and Workman, J.L. (2008). Diverse functions of WD40 repeat proteins in histone recognition. Genes Dev. *22*, 1265–1268.

Tan, J.-Z., Yan, Y., Wang, X.-X., Jiang, Y., and Xu, H.E. (2014). EZH2: biology, disease, and structure-based drug discovery. Acta Pharmacol. Sin. *35*, 161–174.

Tie, F., Banerjee, R., Stratton, C.A., Prasad-Sinha, J., Stepanik, V., Zlobin, A., Diaz, M.O., Scacheri, P.C., and Harte, P.J. (2009). CBP-mediated acetylation of histone H3 lysine 27 antagonizes Drosophila Polycomb silencing. Development *136*, 3131–3141.

Wang, Z., Zang, C., Rosenfeld, J.A., Schones, D.E., Barski, A., Cuddapah, S., Cui, K., Roh, T.-Y., Peng, W., Zhang, M.Q., and Zhao, K. (2008). Combinatorial patterns of histone acetylations and methylations in the human genome. Nat. Genet. *40*, 897–903.

Xu, C., Bian, C., Yang, W., Galka, M., Ouyang, H., Chen, C., Qiu, W., Liu, H., Jones, A.E., MacKenzie, F., et al. (2010). Binding of different histone marks differentially regulates the activity and specificity of polycomb repressive complex 2 (PRC2). Proc. Natl. Acad. Sci. USA *107*, 19266–19271.

Zhang, K., Mosch, K., Fischle, W., and Grewal, S.I.S. (2008). Roles of the Clr4 methyltransferase complex in nucleation, spreading and maintenance of heterochromatin. Nat. Struct. Mol. Biol. *15*, 381–388.

Zheng, Y., He, L., Wan, Y., and Song, J. (2013). H3K9me-enhanced DNA hypermethylation of the p16INK4a gene: an epigenetic signature for spontaneous transformation of rat mesenchymal stem cells. Stem Cells Dev. *22*, 256–267.

Zhu, B., and Reinberg, D. (2011). Epigenetic inheritance: uncontested? Cell Res. *21*, 435–441.

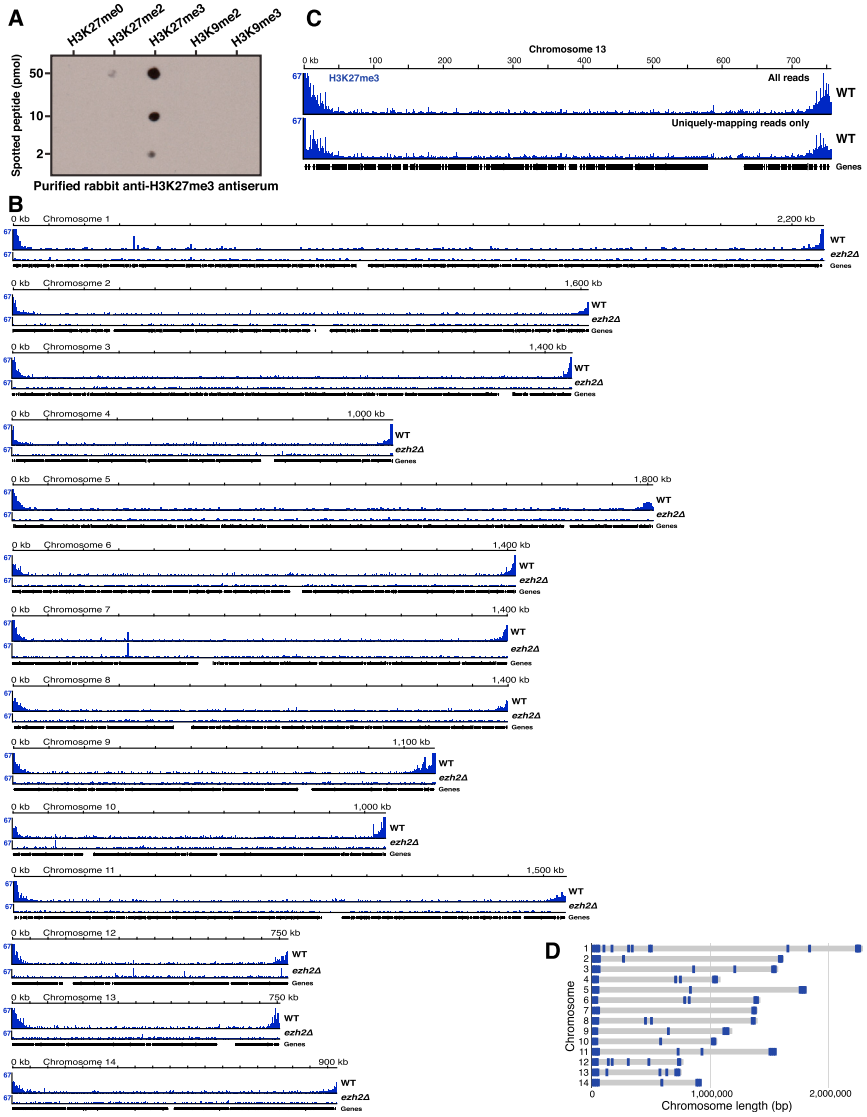

Figure S1. Validation of a Purified Rabbit Antibody for the Detection of *C. neoformans* H3K27me3, Related to Figure 1

(A) Specificity of a purified rabbit antibody against *C. neoformans* H3K27me3. Indicated amounts of synthetic peptides (corresponding to *C. neoformans* histone H3 sequences) were spotted on PVDF and detected by incubation with the rabbit antibody.

(B) ChIP-seq traces of H3K27me3 signal across all *C. neoformans* chromosomes in wild-type and *ezh2Δ* cells. The rDNA repeats have been excluded from analysis.

(C) ChIP-seq traces of H3K27me3 signal across chromosome 13 in wild-type cells. The bottom trace excludes ChIP-seq reads that do not align uniquely to a single site in the genome.

(D) Chromosomal sites at which H3K27me3 signal level reaches > 2.5-fold above background, as measured by ChIP-seq. Any sites at which signal was detected also in an *ezh2Δ* strain have been omitted.

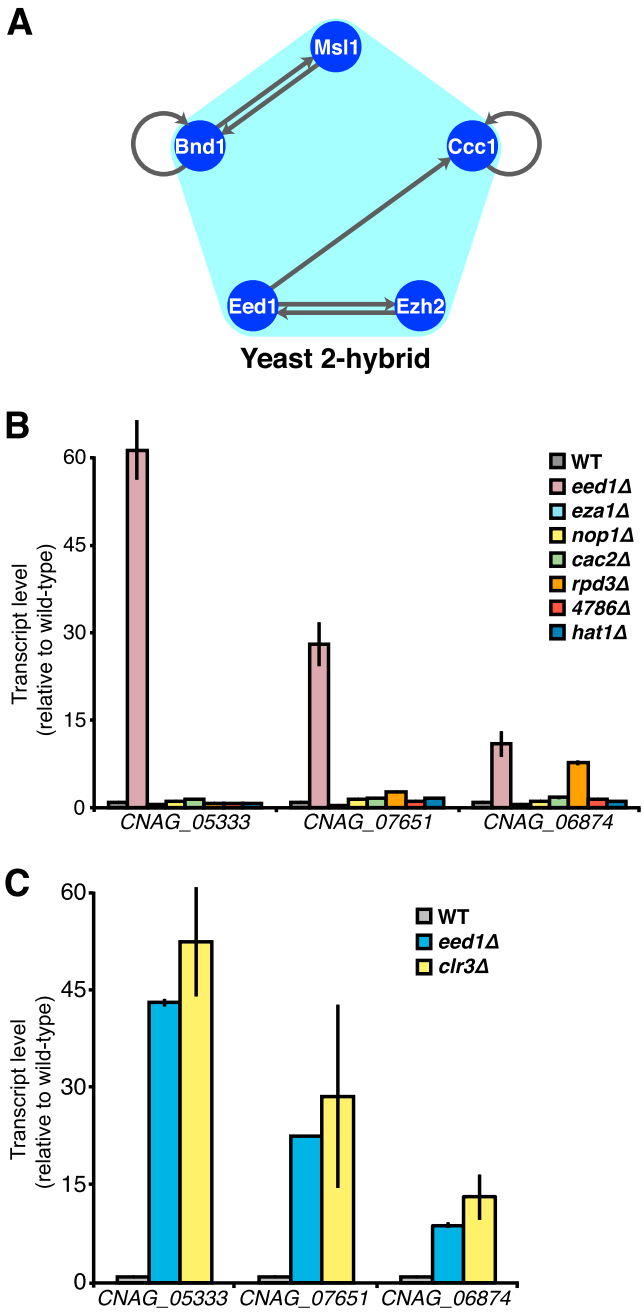

Figure S2. Characterization of Interactions among and Functions of Proteins in the Ezh2 Protein Interaction Network, Related to Figure 2

(A) Protein-protein interactions among PRC2 components, as assessed by yeast two-hybrid assay.

(B) Transcript level of Ezh2 target genes upon loss of Ccc1- and Msl1-associated factors, as assessed by RT-qPCR and normalized to 18S rRNA levels. Error bars represent SD.

(C) Transcript level of Ezh2 target genes upon loss of the Clr3 deacetylase ortholog, as assessed by RT-qPCR and normalized to 18S rRNA levels. Error bars represent SD.

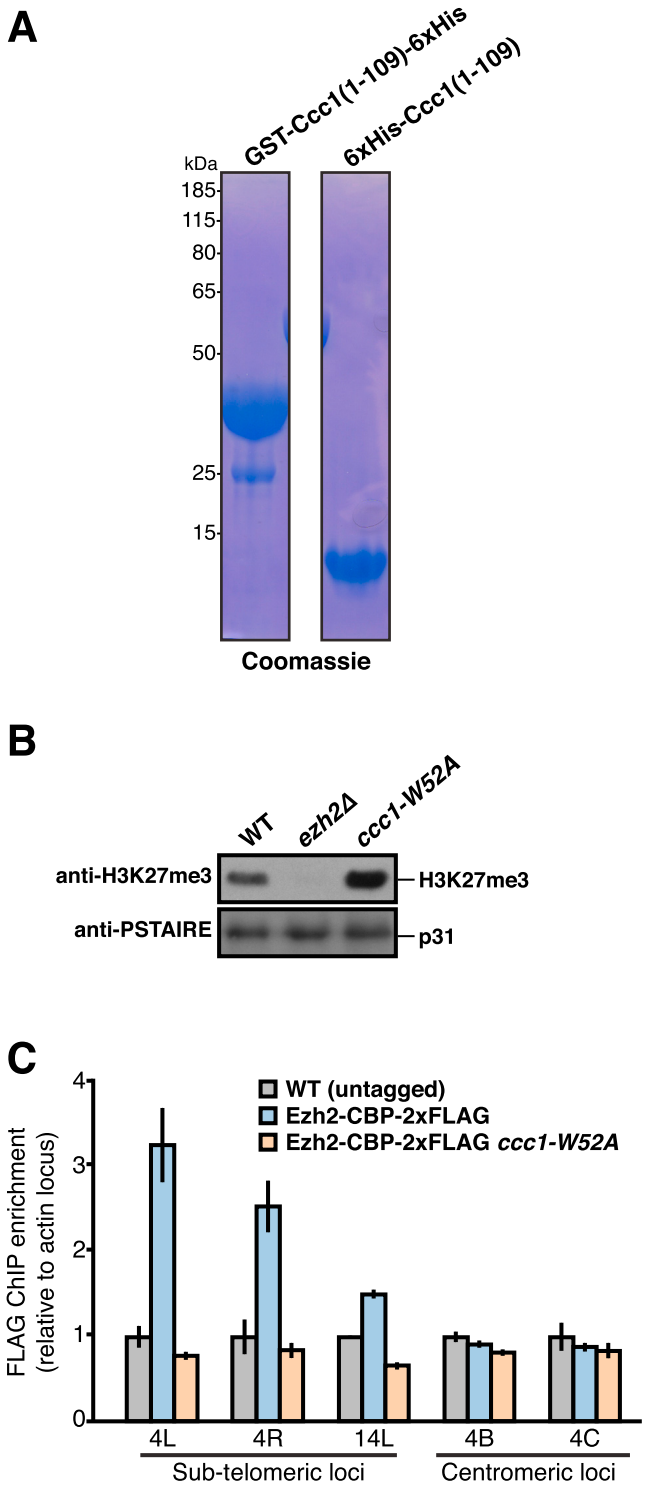

Figure S3. Recombinant Expression of Ccc1 Chromodomain and In Vivo Effects of Its Mutation, Related to Figure 4

(A) Coomassie staining of the Ccc1(1-109) fragment after purification from *E. coli* and resolution by PAGE. GST-tagged protein was used for histone peptide array assay. For fluorescence polarization experiments, the 6xHis-Ccc1(1-109) fragment was used after removal of its His tag.

(B) Levels of H3K27me3 in Ezh2 and Ccc1 mutant cells, as assessed by immunoblot using the antibodies indicated at left. p31 serves as a loading control.

(C) Ezh2-CBP-2xFLAG enrichment at subtelomeric and centromeric loci in the context of Ccc1 chromodomain mutation, as assessed by ChIP-qPCR. Signal was normalized to WCE and to the signal obtained in immunoprecipitations from an untagged strain. Enrichment values are plotted relative to that observed at the euchromatic actin locus. Error bars represent SD.

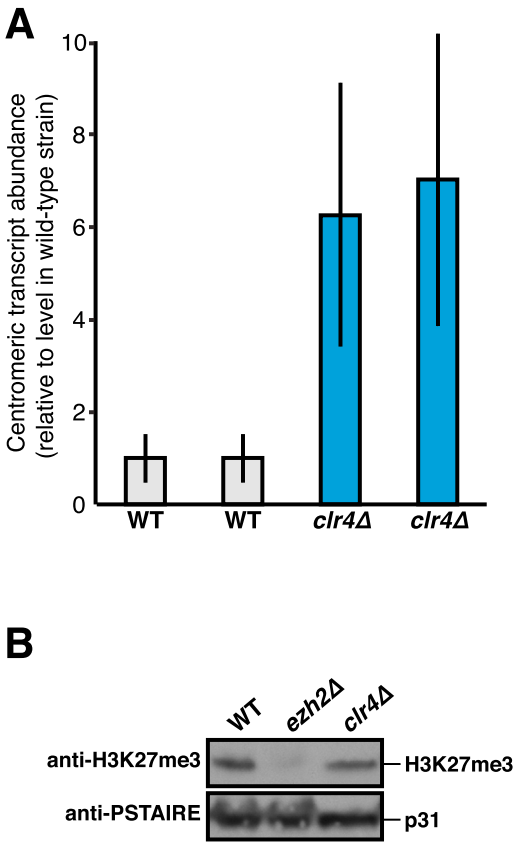

Figure S4. The H3K9 Methyltransferase Clr4 suppresses Centromeric Transcript Accumulation, Related to Figure 5

(A) Centromeric transcript levels in *clr4Δ* cells, as assessed by RNA-seq. For each of the 14 centromeres, overall centromeric transcript level was compared between mutant and wild-type cells. Values reported are the average of all centromeres, normalized to the levels observed in wild-type cells. Error bars represent SD.

(B) Levels of H3K27me3 in *ezh2Δ* and *clr4Δ* cells, as assessed by immunoblot using the antibodies indicated at left. p31 serves as a loading control.

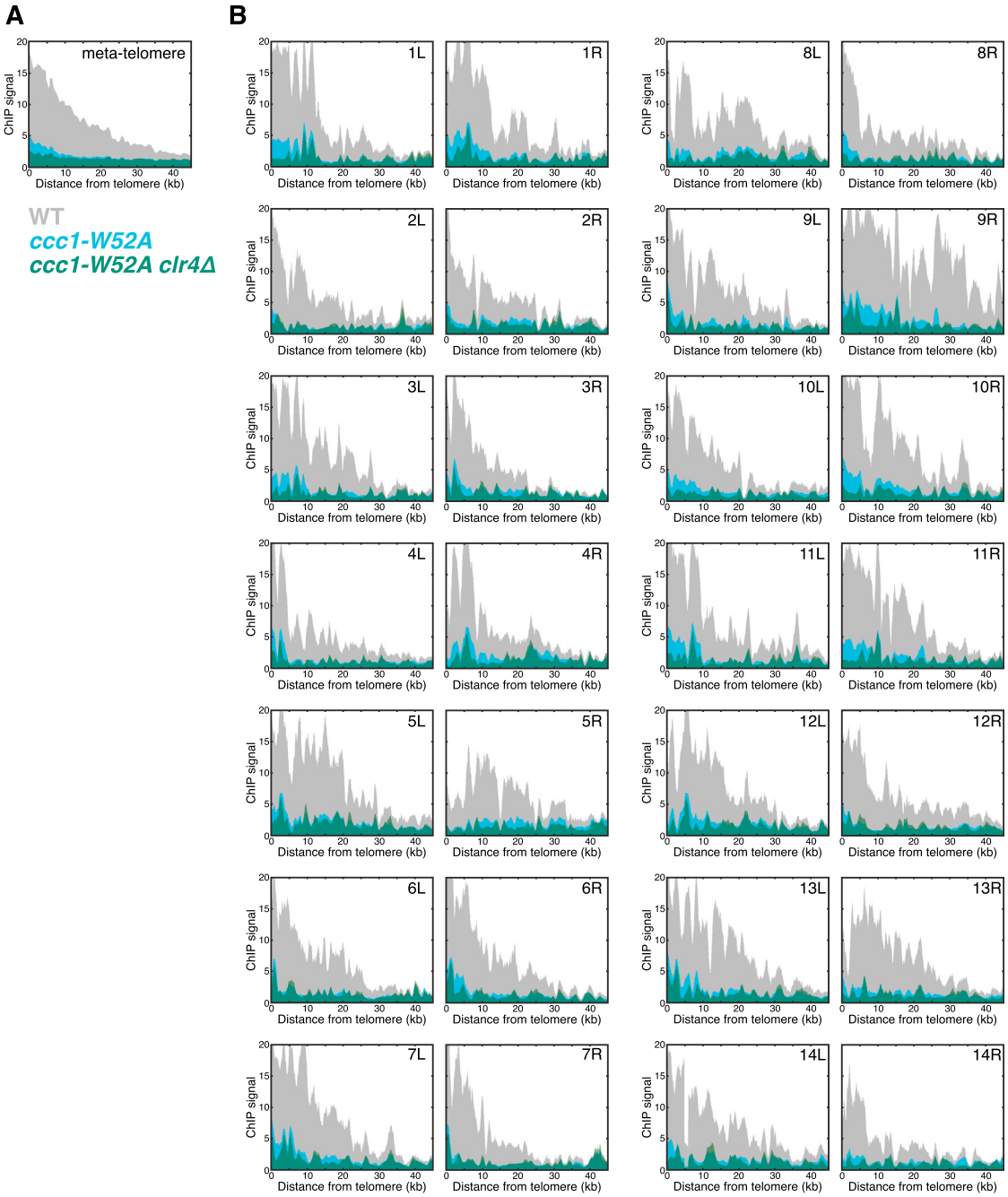

Figure S5. Clr4 Is Required for Subtelomeric H3K27me3 in the *ccc1-W52A* Mutant, Related to Figure 6

(A) Average subtelomeric H3K27me3 signal in *ccc1-W52A* and *ccc1-W52A clr4Δ* cells, as measured by ChIP-seq. ChIP signal at all 28 subtelomeric regions was averaged, normalized to a WCE sample, and plotted as a function of distance from chromosome end.

(B) H3K27me3 signal in *ccc1-W52A* and *ccc1-W52A clr4Δ* cells at each individual subtelomeric region. ChIP signal at each subtelomeric region was normalized to a WCE sample and plotted as a function of distance from chromosome end. Left (L) and right (R) chromosome ends are shown, where left refers to the chromosome end whose terminal base is annotated as position 1.

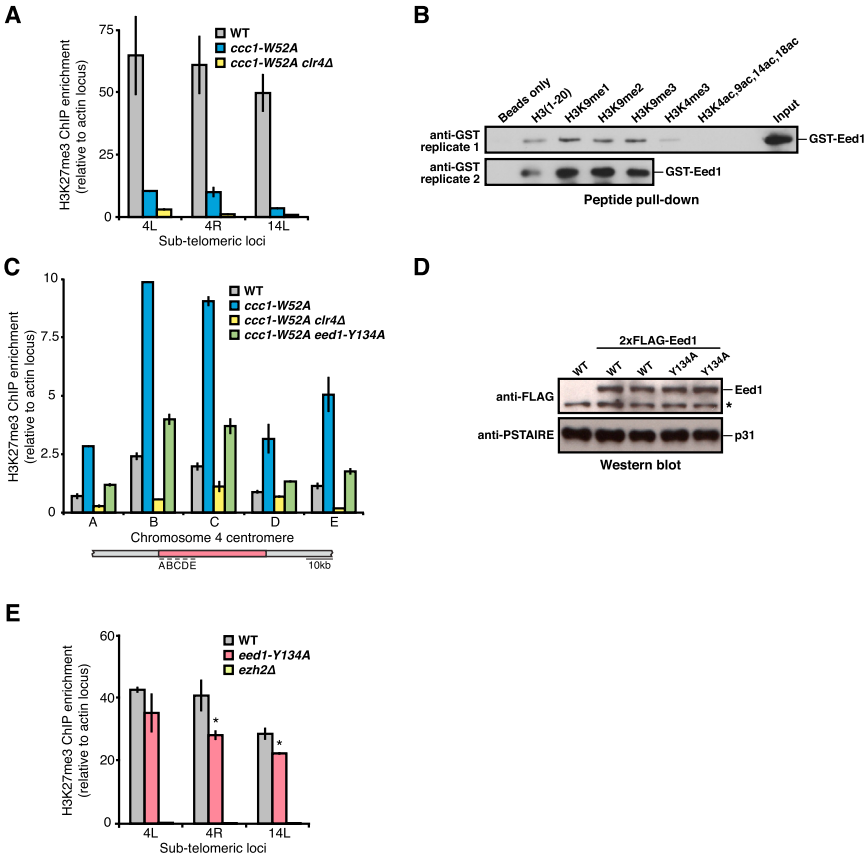

Figure S6. Eed1 Interacts with the Histone H3 N Terminus and Contributes to the Improper Specificity of PRC2 in the Absence of Product Recognition Activity, Related to Figure 6

(A) H3K27me3 enrichment at three subtelomeric loci in the context of Ccc1 chromodomain mutations, as assessed by ChIP-qPCR. Signal was normalized to WCE and is plotted relative to that at the euchromatic actin locus. Error bars represent SD.

(B) Binding of Eed1 with H3(1-20) peptides, as measured by in-solution peptide pull-down assay. Recombinant GST-Eed1 was incubated with peptide-coated magnetic beads and bound protein was detected by immunoblot. Two independent H3K9me1/2/3 experiments are shown.

(C) Effect of Eed1 WD40 domain mutation on the ectopic accumulation of H3K27me3 caused by disruption of Ccc1 chromodomain. H3K27me3 enrichment at five centromeric loci (below) was assessed by ChIP-qPCR. Signal was normalized to WCE and is plotted relative to that at the euchromatic actin locus. Data correspond to the same experiment as Figure 6E. Tyrosine 134 corresponds to tyrosine 148 in human EED. Error bars represent SD.

(D) Expression level of an Eed1 WD40 domain mutant, Y134A, as assessed by immunoblot using the antibodies indicated at left. p31 serves as a loading control. Asterisk indicates a nonspecific band detected by the anti-FLAG antibody.

(E) H3K27me3 enrichment at three subtelomeric loci in the context of Eed1 WD40 domain mutation, as assessed by ChIP-qPCR. Signal was normalized to WCE and is plotted relative to signal at the euchromatic actin locus. Error bars represent SD. Asterisk indicates $p < 0.05$ by Student's t test.